
Conditional Deep Inverse Rosenblatt Transports

Tiangang Cui
School of Mathematics
Monash University
Victoria 3800, Australia
tiangang.cui@monash.edu

Sergey Dolgov
Department of Mathematical Sciences
University of Bath
Bath, BA2 7AY, UK
s.dolgov@bath.ac.uk

Olivier Zahm
Univ. Grenoble Alpes, Inria, CNRS
Grenoble INP, LJK, 38000 Grenoble, France
olivier.zahm@inria.fr

Abstract

We present a novel offline-online method to mitigate the computational burden of the characterization of conditional beliefs in statistical learning. In the offline phase, the proposed method learns the joint law of the belief random variables and the observational random variables in the tensor-train (TT) format. In the online phase, it utilizes the resulting order-preserving conditional transport map to issue real-time characterization of the conditional beliefs given new observed information. Compared with the state-of-the-art normalizing flows techniques, the proposed method relies on function approximation and is equipped with thorough performance analysis. This also allows us to further extend the capability of transport maps in challenging problems with high-dimensional observations and high-dimensional belief variables. On the one hand, we present novel heuristics to reorder and/or reparametrize the variables to enhance the approximation power of TT. On the other, we integrate the TT-based transport maps and the parameter reordering/reparametrization into layered compositions to further improve the performance of the resulting transport maps. We demonstrate the efficiency of the proposed method on various statistical learning tasks in ordinary differential equations (ODEs) and partial differential equations (PDEs).

1 Introduction

Modelling a belief random variable Θ conditioned on available information Y is a fundamental task in statistical learning. Given the law of the joint random variables (Y, Θ) taking values in $\mathbb{R}^{d_Y} \times \mathbb{R}^{d_\Theta}$, the goal is to characterize the conditional belief $\Theta|Y=y$ for some observed information y . Classical inference methods, e.g., Markov chain Monte Carlo [5, 30] and sequential Monte Carlo methods [9, 15], often focus on characterizing the conditional belief given a particular realization of the observed information. In general, these methods rely on *online* computation resources—most of the tasks have to be computed after observing y and have to be repeated for each new set of observations. This strategy may not be suitable for issuing real-time characterizations of conditional beliefs with multiple sets of observed information, because online methods often require a significant amount of computational effort. In this paper, we design an *offline-online* strategy to enable fast characterizations of conditional beliefs for multiple observed information.

Background. In a Bayesian perspective, the joint probability density function (pdf), denoted by $\pi_{Y, \Theta}$, of the random variables (Y, Θ) is defined by the product of the likelihood function $\pi_{Y|\Theta}$ and the

prior π_Θ . This way, given observed information y , the pdf of the conditional belief, or the posterior, is proportional to the joint pdf, i.e., $\pi_{\Theta|Y=y} \propto \pi_{Y,\Theta}(y, \cdot)$. Our ultimate goal is to approximate the joint density $\pi_{Y,\Theta}$ by a density $p_{Y,\Theta} := \mathcal{T}_\# \rho_{Y,\Theta}$, which is defined as the pushforward of some reference product-form density $\rho_{Y,\Theta} = \rho_Y \otimes \rho_\Theta$ on $\mathbb{R}^{d_Y} \times \mathbb{R}^{d_\Theta}$ under an order-preserving map

$$\mathcal{T}(u_Y, u_\Theta) = \begin{bmatrix} \mathcal{T}_Y(u_Y) \\ \mathcal{T}_\Theta(u_Y, u_\Theta) \end{bmatrix}. \quad (1)$$

As suggested by [1, 26, 41], the above triangular structure permits one to easily build *conditional map* $\mathcal{T}_{\Theta|Y=y}(u_\Theta) := \mathcal{T}_\Theta(\mathcal{T}_Y^{-1}(y), u_\Theta)$. This conditional map is such that, for any observed information y , the random variable $\mathcal{T}_{\Theta|Y=y}(U_\Theta)$ with $U_\Theta \sim \rho_\Theta$ follows the approximate conditional pdf $p_{\Theta|Y=y}$. This allows us to devote most of the computational resources to the *offline phase* to learn the map \mathcal{T} , and then rapidly characterize the conditional belief in the *online phase* using the pushforward of the reference ρ_Θ under the conditional map $\mathcal{T}_{\Theta|Y=y}$.

Contribution. We present a novel strategy that learns the map \mathcal{T} from a *function approximation* perspective. Following the work of [11, 16], we employ the tensor-train (TT) decomposition [3, 20, 21, 22] of the joint pdf to explicitly construct an order-preserving map \mathcal{T} and the subsequent conditional map $\mathcal{T}_{\Theta|Y=y}$. For many problems of interests, the joint pdfs can be concentrated to some sub-manifold. Then, the nonlinear interaction and the potential high-dimensionality of variables in the joint pdf can deteriorate the approximation power of the TT decomposition. We propose a combined treatment to overcome this barrier. We first present a novel gradient-based method to reorder and reparametrize the variables to enhance the approximation power of TT. This heuristic relies on the gradient-based dimension reduction technique developed in [12, 13, 45]. Then, we employ the deep inverse Rosenblatt transport (DIRT) framework [11] to decompose the construction of the conditional map into a composition of layers, in which each layer of map is easier to construct.

The function approximation perspective permits the control of the approximation error of the joint pdf in the Hellinger distance

$$\mathcal{D}_H(\pi_{Y,\Theta}, p_{Y,\Theta}) := \left(\frac{1}{2} \int (\sqrt{\pi_{Y,\Theta}} - \sqrt{p_{Y,\Theta}})^2 dy d\theta \right)^{\frac{1}{2}}. \quad (2)$$

The performance of the resulting conditional map is guaranteed with high probability. As shown in Appendix A.2, if $\mathcal{D}_H(\pi_{Y,\Theta}, p_{Y,\Theta}) \leq \varepsilon$ for some $\varepsilon < \sqrt{2}/4$, then the expectation of any quantity of interests $\theta \mapsto h(\theta)$ over the conditional belief has an error satisfying

$$\left| \mathbb{E}_{\pi_{\Theta|Y}}(h) - \mathbb{E}_{p_{\Theta|Y}}(h) \right| \leq \frac{4\varepsilon}{\sqrt{2}\delta - 4\varepsilon} \left(\sqrt{\text{Var}_{\pi_{\Theta|Y}}(h)} + \sqrt{\text{Var}_{p_{\Theta|Y}}(h)} \right), \quad (3)$$

with probability greater than $1 - \delta$ for some $\delta > 2\sqrt{2}\varepsilon$.

Related work. We highlight relevant works in transport maps [1, 4, 26, 37, 43, 44] and normalising flows [6, 7, 10, 27, 36, 38], in which the map is identified by minimizing the Kullback-Leibler (KL) divergence between the target density and its approximation over some class of tractable triangular maps. By and large, these approaches adopt a *density estimation perspective* in which one only has access to samples from the target pdf, and so minimizing the KL divergence boils down to maximum likelihood estimation. In contrast, we build the map using function approximation techniques in which the square root of the density is seen as the function to approximate, and hence the Hellinger distance (2) can be interpreted as an L^2 error. In addition, the access to pointwise evaluations of the density and its gradients enables the gradient-based variable ordering method, which is the key to deploy our method in a high-dimensional context.

Outline. Section 2 presents the TT-based techniques for density approximation. Section 3 introduces a heuristic for variable reordering and reparametrization. Section 4 presents the DIRT-based construction of conditional maps. Section 5 provides numerical experiments. Proofs, derivations, and additional numerical results are provided in Appendix.

2 Single-layered inverse Rosenblatt transform (SIRT)

A central element of our method is the TT-based approximation to the joint density,

$$p_{Y,\Theta}(y, \theta) \propto g(y, \theta)^2, \quad (4)$$

where g is an unnormalized approximation to $\sqrt{\pi_{Y,\Theta}}$ in the TT format

$$g(y, \theta) = \mathcal{G}_{-d_Y}(y_{d_Y}) \dots \mathcal{G}_{-1}(y_1) \mathcal{G}_1(\theta_1) \dots \mathcal{G}_{d_\Theta}(\theta_{d_\Theta}). \quad (5)$$

Here, each $\mathcal{G}_k : \mathbb{R} \rightarrow \mathbb{R}^{r_{k-1} \times r_k}$ is a matrix-valued function called the k -th TT core and $\text{rank}_{\text{TT}}(g) = (r_{-d_Y-1}, \dots, r_{d_\Theta})$ gives the TT ranks of g . We set $r_{-d_Y-1} = r_{d_\Theta} = 1$ and use the convention $r_{-1} = r_0$. The TT decomposition (5) can be built by alternating-direction TT-Cross approximation methods [19, 31, 34]. Following [17], these methods can adapt the TT rank of g to reach a desired error threshold ε so that $\|\sqrt{\pi_{Y,\Theta}} - g\|_2 \leq \varepsilon/\sqrt{2}$, where $\|\cdot\|_2$ denotes the L^2 -norm. As shown in Appendix B.1, the TT approximation yields a controlled error in the approximate pdf, $\mathcal{D}_{\text{H}}(\pi_{Y,\Theta}, p_{Y,\Theta}) \leq \varepsilon$, in the Hellinger distance.

The approximation (4) offers twofold benefits. First, the approximate joint density is non-negative by construction. Second, the TT format enables explicit integration of g^2 dimension-by-dimension. This permits the computation of the normalizing constant $\int g(y, \theta)^2 dy d\theta$ of the unnormalized density in (4) and, more interestingly, the construction of the conditional cumulative density functions (cdfs)

$$F_{Y_k|Y_{>k}}(y_k|y_{>k}) = \int_{-\infty}^{y_k} p_{Y_k|Y_{>k}}(t|y_{>k}) dt, \quad (6)$$

$$F_{\Theta_k|Y, \Theta_{<k}}(\theta_k|\theta_{<k}, y) = \int_{-\infty}^{\theta_k} p_{Y, \Theta_k|\Theta_{<k}}(t|\theta_{<k}, y) dt. \quad (7)$$

This leads to the Rosenblatt transport $\mathcal{F} : \mathbb{R}^{d_Y+d_\Theta} \rightarrow [0, 1]^{d_Y+d_\Theta}$ defined by $\mathcal{F}(y, \theta) = [\mathcal{F}_Y(y), \mathcal{F}_\Theta(y, \theta)]^\top$ where

$$\mathcal{F}_Y(y) = \begin{pmatrix} F_{Y_{d_Y}}(y_{d_Y}) \\ F_{Y_{d_Y-1}|Y_{d_Y}}(y_{d_Y-1}|y_{d_Y}) \\ \vdots \\ F_{Y_1|Y_{>1}}(y_1|y_{>1}) \end{pmatrix} \quad \text{and} \quad \mathcal{F}_\Theta(y, \theta) = \begin{pmatrix} F_{\Theta_1|Y}(\theta_1|y) \\ F_{\Theta_2|Y, \Theta_1}(\theta_2|y, \theta_1) \\ \vdots \\ F_{\Theta_{d_\Theta}|Y, \Theta_{<d_\Theta}}(\theta_{d_\Theta}|y, \theta_{<d_\Theta}) \end{pmatrix}. \quad (8)$$

The Rosenblatt transport is such that $\mathcal{F}_\# p_{Y,\Theta} = \mu_{Y,\Theta}$, where $\mu_{Y,\Theta}$ is the pdf of the uniform measure on the unit hypercube $[0, 1]^{d_Y+d_\Theta}$. Thus, the inverse of the Rosenblatt transport $\mathcal{T} = \mathcal{F}^{-1}$ is a lower-triangular map as in (1) that satisfies $\mathcal{T}_\# \mu_{Y,\Theta} = p_{Y,\Theta}$. More generally, given an arbitrary product-form pdf $\rho_{Y,\Theta}(y, \theta) = \prod_{i=1}^{d_Y} \rho_{Y_i}(y_i) \prod_{j=1}^{d_\Theta} \rho_{\Theta_j}(\theta_j)$, the map $\mathcal{T} = \mathcal{F}^{-1} \circ \mathcal{R}$ satisfies $\mathcal{T}_\# \rho_{Y,\Theta} = p_{Y,\Theta}$ where \mathcal{R} denotes the diagonal Rosenblatt transport of $\rho_{Y,\Theta}$ such that $\mathcal{R}_\# \rho_{Y,\Theta} = \mu_{Y,\Theta}$. Notice that \mathcal{T} is a composition of lower-triangular maps that preserves the lower-triangular structure in (1).

In the *offline phase*, we construct SIRT by computing all the conditional cdfs. See Appendix B.2 for detailed derivations and Algorithm 1 for a summary of the procedure. Denoting the maximum TT rank by r , $\mathcal{O}((d_Y+d_\Theta)r^2)$ number of joint density evaluations and an additional $\mathcal{O}((d_Y+d_\Theta)r^3)$ floating point operations (flops) are needed to build the TT decomposition. It costs another $\mathcal{O}((d_Y+d_\Theta)r^3)$ flops to construct all the marginal cdfs. In the *online phase*, for given observed data y , the conditional map based on SIRT is given by $\mathcal{T}_{\Theta|Y=y} := \mathcal{F}_\Theta^{-1}(\mathcal{F}_Y(y), \cdot)$. Evaluating the conditional map for each given u costs $\mathcal{O}(d_\Theta r^2)$ flops.

Algorithm 1 Single-layered Inverse Rosenblatt Transform (SIRT).

- 1: **procedure** SIRT($\rho_{Y,\Theta}, \pi_{Y,\Theta}, \varepsilon$)
 - 2: Approximate $\sqrt{\pi_{Y,\Theta}}$ by a TT decomposition g as in (5) such that $\|\sqrt{\pi_{Y,\Theta}} - g\|_2 \leq \varepsilon/\sqrt{2}$.
 - 3: Compute the conditional cdfs (6) and (7).
 - 4: Assemble the Rosenblatt transport $\mathcal{F} : \mathbb{R}^d \rightarrow [0, 1]^d$ as in (8).
 - 5: Assemble the diagonal Rosenblatt transport $\mathcal{R} : \mathbb{R}^d \rightarrow [0, 1]^d$ such that $\mathcal{R}_\# \rho_{Y,\Theta} = \mu_{Y,\Theta}$.
 - 6: **return** the lower-triangular map $\mathcal{T} = \mathcal{F}^{-1} \circ \mathcal{R}$ that satisfies $\mathcal{D}_{\text{H}}(\mathcal{T}_\# \rho_{Y,\Theta}, \pi_{Y,\Theta}) \leq \varepsilon$.
 - 7: **end procedure**
-

Remark 1. The regularity of \mathcal{T} actually depends on g : \mathcal{T} might have unbounded derivative around locations where g is close to zero. One way to avoid this is to enforce the approximate joint density to be strictly positive. For a pdf supported on a bounded domain, this can be achieved by considering $p_{Y,\Theta}(y, \theta) \propto g(y, \theta)^2 + \gamma$ for some $\gamma > 0$ rather than (4). See [11] for further details.

3 Variable reordering and reparametrization

The efficiency of TT decompositions strongly depends on the variable ordering. We propose to reorder the variables so that the most *interdependent* variables are placed in the middle of the TT approximation, whereas the rest of *mutually independent* variables are placed in the tails of TT. The rationale behind this is the following: for some $n_\Theta < d_\Theta$ and $n_Y < d_Y$, if the variables $\Theta_{n_\Theta+1}, \dots, \Theta_{d_\Theta}, Y_{n_Y+1}, \dots, Y_{d_Y}$ and the block of variables $(\Theta_{\leq n_\Theta}, Y_{\leq n_Y})$ are all mutually independent, then the pdf $\pi_{Y,\Theta}$ can be equivalently expressed in a factorized form of

$$\tilde{\pi}_{Y,\Theta}(y, \theta) = \left(\prod_{i=n_Y+1}^{d_Y} \tilde{\pi}_{Y_i}(y_i) \right) \tilde{\pi}_{Y_{\leq n_Y}, \Theta_{\leq n_\Theta}}(y_{\leq n_Y}, \theta_{\leq n_\Theta}) \left(\prod_{j=n_\Theta+1}^{d_\Theta} \tilde{\pi}_{\Theta_j}(\theta_j) \right). \quad (9)$$

In this case, $g \approx (\tilde{\pi}_{Y,\Theta})^{1/2}$ admits $\text{rank}_{\text{TT}}(g) = (1, \dots, 1, r_{-n_Y-1}, \dots, r_{n_\Theta}, 1, \dots, 1)$. In practice, $\pi_{Y,\Theta}$ might not have such a mutual independence structure. Instead, it can have a *low-dependency structure*, in the sense that $\pi_{Y,\Theta}$ can be accurately approximated by a pdf $\tilde{\pi}_{Y,\Theta}$ structured as in (9). In this case, we expect the TT decomposition g to have small ranks in its left and right tails.

To detect the low-dependency structure in $\pi_{Y,\Theta}$, we define a product-form reference pdf

$$\rho_{Y,\Theta}(y, \theta) = \rho_Y(y) \rho_\Theta(\theta), \quad \text{where } \rho_Y(y) = \prod_{i=1}^{d_Y} \pi_{Y_i | \Theta = \theta_0}(y_i) \text{ and } \rho_\Theta(\theta) = \prod_{j=1}^{d_\Theta} \pi_{\Theta_j}(\theta_j), \quad (10)$$

for some arbitrary $\theta_0 \in \mathbb{R}^{d_\Theta}$, e.g., the prior mean in our numerical experiments. Then, the matrices

$$H_Y = \int \left(\nabla_y \log \frac{\pi_{Y,\Theta}}{\rho_{Y,\Theta}} \right) \left(\nabla_y \log \frac{\pi_{Y,\Theta}}{\rho_{Y,\Theta}} \right)^\top d\pi_{Y,\Theta}, \quad (11)$$

$$H_\Theta = \int \left(\nabla_\theta \log \frac{\pi_{Y,\Theta}}{\rho_{Y,\Theta}} \right) \left(\nabla_\theta \log \frac{\pi_{Y,\Theta}}{\rho_{Y,\Theta}} \right)^\top d\pi_{Y,\Theta}, \quad (12)$$

contain exploitable information regarding the distance between $\pi_{Y,\Theta}$ and $\rho_{Y,\Theta}$. For instance, $\text{trace}(H_\Theta) + \text{trace}(H_Y) = \mathbb{E}_{\pi_{Y,\Theta}}[\|\nabla \log \pi_{Y,\Theta} - \nabla \log \rho_{Y,\Theta}\|^2]$ is the *relative Fisher information* that can bound the KL divergence $\mathcal{D}_{\text{KL}}(\pi_{Y,\Theta} \| \rho_{Y,\Theta})$, see [35]. The following proposition offers a viable path to reordering variables according to the diagonals of H_Θ and H_Y .

Proposition 1. *Assume $\rho_{Y,\Theta}$ satisfies the Poincaré inequality, i.e., there exists a constant $\kappa < \infty$ so that $\text{Var}_{\rho_{Y,\Theta}}(h) \leq \kappa \mathbb{E}_{\rho_{Y,\Theta}}(\|\nabla h\|_2^2)$ holds for any sufficiently smooth function $h : \mathbb{R}^{d_\Theta+d_Y} \rightarrow \mathbb{R}$. Then, for any $n_Y \leq d_Y$ and $n_\Theta \leq d_\Theta$, there exists a lower-dimensional density function $\tilde{\pi}_{Y_{\leq n_Y}, \Theta_{\leq n_\Theta}} : \mathbb{R}^{n_Y+n_\Theta} \rightarrow \mathbb{R}$ that yields an approximation*

$$\tilde{\pi}_{Y,\Theta}(y, \theta) = \left(\prod_{i=n_Y+1}^{d_Y} \rho_{Y_i}(y_i) \right) \tilde{\pi}_{Y_{\leq n_Y}, \Theta_{\leq n_\Theta}}(y_{\leq n_Y}, \theta_{\leq n_\Theta}) \left(\prod_{j=n_\Theta+1}^{d_\Theta} \rho_{\Theta_j}(\theta_j) \right), \quad (13)$$

of the form (9) that satisfies

$$\mathcal{D}_{\text{H}}(\pi_{Y,\Theta}, \tilde{\pi}_{Y,\Theta})^2 \leq \frac{\kappa}{4} \left(\sum_{i=n_Y+1}^{d_Y} (H_Y)_{ii} + \sum_{j=n_\Theta+1}^{d_\Theta} (H_\Theta)_{jj} \right). \quad (14)$$

The proof is given in Appendix C.2. This proposition suggests to sort the variables $\theta_1, \dots, \theta_{d_\Theta}$ and y_1, \dots, y_{d_Y} such that $i \mapsto (H_Y)_{ii}$ and $j \mapsto (H_\Theta)_{jj}$ are decreasing. This way, the right-hand-side of (14) is minimized for any n_Y, n_Θ . This proposition also suggests that one only needs to build the TT decomposition of $\tilde{\pi}_{Y_{\leq n_Y}, \Theta_{\leq n_\Theta}}$ after truncating the variables Y and Θ to the first n_Y and n_Θ components, while controlling the resulting truncation error. In Appendix C.3, we also provide a closed form expression for the optimal $\tilde{\pi}_{Y,\Theta}$ as in (13) that minimizes the Hellinger error.

In addition to variable reordering, we can also reparametrize the variables y and θ to further enhance the approximation power of TT. To preserve the product structure of the reference density in (10) after reparametrization, we restrict the analysis to Gaussian prior π_Θ and Gaussian likelihood $\pi_{Y|\Theta}$.

Proposition 2. Assume the joint density takes the form

$$\pi_{Y,\Theta}(y, \theta) \propto \exp\left(-\frac{1}{2}\|y - G(\theta)\|_2^2 - \frac{1}{2}\|\theta - \theta_0\|_2^2\right), \quad (15)$$

where $\theta \mapsto G(\theta) \in \mathbb{R}^{d_Y}$ is a smooth forward operator and $\|\cdot\|_2$ the Euclidean norm¹. Let $A \in \mathbb{R}^{d_Y \times d_Y}$ and $B \in \mathbb{R}^{d_\Theta \times d_\Theta}$ be unitary matrices containing the eigenvectors of H_Y and H_Θ in the decreasing order, respectively. Then there exists a pdf $\tilde{\pi}_{Y,\Theta}^{A,B}(y, \theta) = \tilde{\pi}_{Y,\Theta}(A^\top y, B^\top \theta)$, with $\tilde{\pi}_{Y,\Theta}$ as in (13) such that

$$\mathcal{D}_H(\pi_{Y,\Theta}, \tilde{\pi}_{Y,\Theta}^{A,B})^2 \leq \frac{1}{4} \left(\sum_{i=n_Y+1}^{d_Y} \lambda_i(H_Y) + \sum_{i=n_\Theta+1}^{d_\Theta} \lambda_i(H_\Theta) \right), \quad (16)$$

holds for any $n_Y \leq d_Y$ and $n_\Theta \leq d_\Theta$, where $\lambda_i(\cdot)$ denotes the i -th largest eigenvalue.

The proof is given in Appendix C.4. Proposition 2 suggests to reparametrize Y and Θ using the dominant eigenvectors of H_Y and H_Θ , respectively. As shown in Appendix C.5, the Gaussian assumption in (15) leads to the matrices

$$H_Y \stackrel{(11)\&(15)}{=} \int (G(\theta) - G(\theta_0))(G(\theta) - G(\theta_0))^\top d\pi_\Theta \quad \text{and} \quad H_\Theta \stackrel{(12)\&(15)}{=} \int \nabla G(\theta)^\top \nabla G(\theta) d\pi_\Theta.$$

Thus, the principal components of the model outputs $G(\Theta)$ are used to reparametrize Y and the directions in which the linearized forward model varies the most are used to reparametrize Θ .

4 Deep inverse Rosenblatt transform (DIRT)

For target pdfs that are concentrated to a small subdomain or have complicated correlation structures, it can be challenging to construct in one step a TT approximation to $\sqrt{\pi_{Y,\Theta}}$. DIRT alleviates this difficulty by building a composition of transport maps

$$\mathcal{T}_L = \mathcal{Q}_0 \circ \mathcal{Q}_1 \circ \dots \circ \mathcal{Q}_L,$$

guided by a sequence of bridging pdfs

$$\pi_{Y,\Theta}^0, \pi_{Y,\Theta}^1, \dots, \pi_{Y,\Theta}^L := \pi_{Y,\Theta},$$

with increasing complexity. For example, using the tempering technique [18, 33, 42], one may consider the bridging pdfs $\pi_{Y,\Theta}^\ell \propto \varphi_{Y,\Theta}^{\beta_\ell} \rho_{Y,\Theta}$, where $\varphi_{Y,\Theta} = \pi_{Y,\Theta} / \rho_{Y,\Theta}$ and $0 = \beta_0 \leq \beta_1 \leq \dots \leq \beta_L = 1$ are some chosen temperatures and $\rho_{Y,\Theta}$ as in (10).

We propose to build the layers $\mathcal{Q}_0, \dots, \mathcal{Q}_L$ in a greedy way. For each $0 \leq \ell \leq L$, the composed map $\mathcal{T}_\ell = \mathcal{Q}_0 \circ \dots \circ \mathcal{Q}_\ell$ yields an approximation $p_{Y,\Theta}^\ell := (\mathcal{T}_\ell)_\# \rho_{Y,\Theta}$ to the bridging pdf $\pi_{Y,\Theta}^\ell$. At each greedy iteration, $\mathcal{Q}_{\ell+1}$ is constructed as a SIRT so that the new pushforward density $p_{Y,\Theta}^{\ell+1} = (\mathcal{T}_\ell \circ \mathcal{Q}_{\ell+1})_\# \rho_{Y,\Theta}^\ell$ approximates the next bridging density $\pi_{Y,\Theta}^{\ell+1}$ in a way that

$$\mathcal{D}_H(p_{Y,\Theta}^{\ell+1}, \pi_{Y,\Theta}^{\ell+1}) \leq \omega \mathcal{D}_H(p_{Y,\Theta}^\ell, \pi_{Y,\Theta}^{\ell+1}),$$

for some relative error bound $\omega < 1$. This is equivalent to

$$\mathcal{D}_H((\mathcal{Q}_{\ell+1})_\# \rho_{Y,\Theta}, \mathcal{T}_\ell^\# \pi_{Y,\Theta}^{\ell+1}) \leq \omega \mathcal{D}_H(\rho_{Y,\Theta}, \mathcal{T}_\ell^\# \pi_{Y,\Theta}^{\ell+1}). \quad (17)$$

The following proposition shows the convergence of the greedy construction of DIRT.

Proposition 3. Assume there exists a constant $\eta(L) < 1$ such that the bridging pdfs satisfy

$$\sup_{0 \leq \ell < L} \mathcal{D}_H(\pi_{Y,\Theta}^\ell, \pi_{Y,\Theta}^{\ell+1}) = \eta(L). \quad (18)$$

Furthermore, assume there exists $\omega < 1$ so that $\mathcal{Q}_1, \dots, \mathcal{Q}_L$ satisfy (17) for any ℓ and assume that the initial map \mathcal{Q}_0 satisfies $\mathcal{D}_H((\mathcal{Q}_0)_\# \rho_{Y,\Theta}, \pi_{Y,\Theta}^0) \leq \omega \eta(L)$. Then the resulting composite map $\mathcal{T}_L = \mathcal{Q}_0 \circ \mathcal{Q}_1 \circ \dots \circ \mathcal{Q}_L$ defines a pushforward density $p_{Y,\Theta} = (\mathcal{T}_L)_\# \rho_{Y,\Theta}$ that satisfies

$$\mathcal{D}_H(p_{Y,\Theta}, \pi_{Y,\Theta}) \leq \frac{\omega}{1-\omega} \eta(L). \quad (19)$$

¹For problems equipped with non-Euclidean norms (*i.e.* non-identity covariance matrices) one can apply whitening transforms so that the results of this proposition still holds. See Appendix C.5.

The proof is given in Appendix D.1. Under mild assumptions, Appendix D.2 shows that tempered bridging densities $\pi_{Y,\Theta}^\ell \propto \varphi_{Y,\Theta}^{\beta_\ell} \rho_{Y,\Theta}$ with uniformly spaced temperatures $\beta_\ell = \ell/L$ satisfy (18) with $\eta(L) = \mathcal{O}(1/L)$. Algorithm 2 details the construction of DIRT with a controlled error, in which each layer of the composition $\mathcal{Q}_{\ell+1}$ is constructed using the SIRT Algorithm 1. The resulting map \mathcal{T}_L is lower-triangular as a composition of lower-triangular maps. In addition, the temperatures β_ℓ can be adaptively chosen during the greedy procedure in order to ensure $\mathcal{D}_H(\pi_{Y,\Theta}^\ell, \pi_{Y,\Theta}^{\ell+1}) \leq \eta$ for some prescribed $\eta < 1$, see Appendix D.3 for additional details.

Algorithm 2 Deep Inverse Rosenblatt Transform (DIRT).

- 1: **procedure** DIRT($\rho_{Y,\Theta}, \{\pi_{Y,\Theta}^\ell\}_{\ell=1}^L, \varepsilon$) $\triangleright \varepsilon \leq \omega\eta(L)$
 - 2: Call SIRT($\rho_{Y,\Theta}, \pi_{Y,\Theta}^0, \varepsilon$) to get the first layer \mathcal{Q}_0 and initialize $\mathcal{T}_0 = \mathcal{Q}_0$.
 - 3: **for** $\ell = 0, \dots, L - 1$ **do**
 - 4: Call SIRT($\rho_{Y,\Theta}, \mathcal{T}_\ell^\# \pi_{Y,\Theta}^{\ell+1}, \varepsilon$) to get the next layer $\mathcal{Q}_{\ell+1}$ and update $\mathcal{T}_{\ell+1} = \mathcal{T}_\ell \circ \mathcal{Q}_{\ell+1}$.
 - 5: **end for**
 - 6: **return** the lower-triangular map \mathcal{T}_L that satisfies $\mathcal{D}_H((\mathcal{T}_L)_\# \rho_{Y,\Theta}, \pi_{Y,\Theta}) \leq \frac{\omega}{1-\omega} \eta(L)$.
 - 7: **end procedure**
-

5 Numerical examples

SIR: comparison to neural network transport. The Susceptible-Infected-Recovered model is a system of ODEs

$$\frac{dS(t)}{dt} = -\beta SI, \quad \frac{dI(t)}{dt} = \beta SI - \gamma I, \quad \frac{dR(t)}{dt} = \gamma I, \quad (20)$$

started from $S(0) = 99, I(0) = 1, R(0) = 0$, and solved using ode45 in Matlab with a relative error threshold 10^{-6} . The parameters $\theta = (\beta, \gamma)$ are subject to inference from the posterior distribution, conditional on 4 noisy observations of the number of infected individuals. The latter are modelled as

$$y = (I(1.25), I(2.5), I(3.75), I(5)) + e^y, \quad \text{where } e_i^y \sim \mathcal{N}(0, 1), \quad i = 1, \dots, 4. \quad (21)$$

Reasonable values of β and γ vary between 0 and 2, so we use a uniform prior $\pi_\Theta = \mu_{[0,2]^2}$. The total initial number of individuals of 100 yields y in the range $[0, 100]$.

Therefore, in the initial DIRT layer, we introduce 17 equispaced discretization points on $[0, 2]$ for θ_1, θ_2 , and 17 equispaced discretization points on $[0, 100]$ for y_1, \dots, y_4 . We set the TT ranks to 17, the reference measure to the truncated normal distribution on $[-3, 3]$, and the tempering powers starting from $\beta_0 = 10^{-4}$ and increasing geometrically as $\beta_{\ell+1} = \sqrt{10} \cdot \beta_\ell$ until $\beta_8 = 1$. Constructing DIRT with those parameters requires a total of 182070 evaluations of the bridging densities in all layers, and 21 seconds of CPU time in Matlab R2020a on an Intel Core i7-9750H CPU. Since we are mostly interested in sampling from the posterior rather than the joint, the accuracy of the DIRT approximation is benchmarked as follows. We sample 256 realisations of $\Theta \sim \pi_\Theta$ and $e^y \sim \mathcal{N}(0, \text{Id})$. By solving the ODE model (20) for each Θ adding the corresponding e^y as in (21), we generate 256 realizations of synthetic data.

Then, we plug each data set y^i into the conditional DIRT to obtain a resulting approximate posterior density $p_{\Theta|Y=y^i}$ and draw $N = 5 \cdot 10^4$ number of conditional random variables $\Theta|Y=y^i$ from each $p_{\Theta|Y=y^i}$. Producing one conditional sample from DIRT takes 43 microseconds of CPU time. These samples are used to estimate the Hellinger distance between the approximate posterior density $p_{\Theta|Y=y^i}$ and the exact posterior density $\pi_{\Theta|Y=y^i}$. The 256 instances of the Hellinger distances, corresponding to the different realizations of Y , are binned in a histogram as shown in Figure 1 (top left). We observe that although conditioning the approximate joint pdf on the tail of the data distribution might result in a rather large relative error in the DIRT-approximation of the corresponding conditional density, such outliers are rare. This behaviour is expected as the Hellinger error of the approximate conditional density is controlled with high probability in our framework.

We also compare DIRT with the Hierarchical Invertible Neural Transport (HINT) [27] in this example. HINT approximates a transport map using iid samples drawn from the joint pdf that can be generated

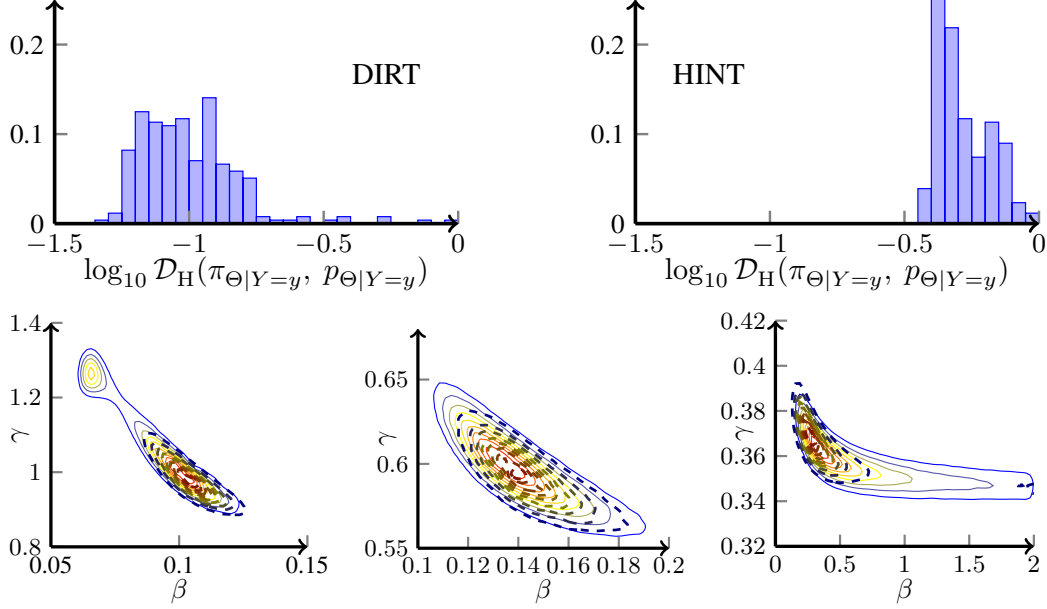


Figure 1: Top: frequencies (out of 256 experiments with different y) of Hellinger distances between exact and approximate posterior distributions for DIRT (left) and HINT (right). Bottom: posterior density approximations for three realisations of y for DIRT (solid lines) and HINT (dashed lines).

explicitly in this case. Inverting this map conditioned on a particular value of y gives samples from the approximate posterior. The HINT map is constructed from neural networks with 8 dense layers of size 200×200 each, trained by 50 epochs of 10^6 training samples. The training took 28 minutes on a NVidia GeForce GTX 1650 Max-Q card, and the evaluation of one test sample took 13 microseconds. A histogram of Hellinger-distance errors in the HINT approximation of the posterior is shown on Figure 1 (top right). We see that DIRT is systematically more accurate than HINT despite using an order of magnitude less training evaluations of the forward model and time.

The bottom row of Figure 1 shows the contours of various approximate posterior densities conditioned on three different data realizations. The bottom left plot of Figure 1 shows an interesting multimodal posterior distribution, in which the “true” parameter $\theta = (0.1, 1)$ is used to generate the synthetic data. This corresponds to a realistic balance between infection and recovery rates. For this test case, DIRT gives the Hellinger distance $\mathcal{D}_H(\pi_{\Theta|Y=y}, p_{\Theta|Y=y}) \approx 0.32$, whereas HINT gives $\mathcal{D}_H(\pi_{\Theta|Y=y}, p_{\Theta|Y=y}) \approx 0.68$.

Wrenchmark [28, 40]. We consider a two-dimensional linear elasticity problem that models the displacement field $u : \mathcal{D} \rightarrow \mathbb{R}^2$ using the PDE $\text{div}(K : \varepsilon(u)) = f$ on $\mathcal{D} \subset \mathbb{R}^2$. Here, $\varepsilon(u) = \frac{1}{2}(\nabla u + \nabla u^\top)$ is the strain field, and K is the Hooke tensor given by $K : \varepsilon(u) = \frac{E}{1+\nu}\varepsilon(u) + \frac{\nu E}{1-\nu^2}\text{trace}(\varepsilon(u))\begin{pmatrix} 1 & 0 \\ 0 & 1 \end{pmatrix}$, where $\nu = 0.3$ is the Poisson’s ratio and $E > 0$ is the Young’s modulus. In this example, the Young’s modulus $E : \mathcal{D} \rightarrow \mathbb{R}_{>0}$ is the belief variable we want to estimate. It is modelled by a random field that follows a log-normal prior $\log E \sim \mathcal{N}(0, C)$, where $C(s, t) = \exp(-\|s - t\|_2^2)$ is a Gaussian covariance function on $\mathcal{D} \times \mathcal{D}$. After finite element discretization, $\log E$ is replaced with a piecewise constant field whose elementwise values are gathered in a vector $\theta \in \mathbb{R}^{d_\Theta}$ where $d_\Theta = 925$ is the number of elements in the mesh. The parameter θ thus follows a centered Gaussian prior with covariance matrix $\Sigma_{ij} = C(s_i, s_j)$, where $s_i \in \mathcal{D}$ is the center of the i -th element. We compute the numerical solution $u^h = u^h(\theta)$ by the Galerkin projection of $u = u(\theta)$ onto the space of continuous piecewise affine functions over a triangular mesh. The domain \mathcal{D} , the mesh, the boundary conditions, and a sample von Mises stress of the solution are shown in Figure 2 (middle).

We observe the vertical displacements u_2^h of the 26 points of interests located along the green line where the force f is applied, see Figure 2 (middle). The perturbed observations are $y = u_2^h + e$

where e is a zero-mean H^1 -normal noise with the signal-to-noise-ratio 10. Following Proposition 2, we reparametrize and truncate both θ and y by replacing them with $\theta_{\leq n_\Theta} = B_{n_\Theta}^\top \theta \in \mathbb{R}^{n_\Theta}$ and $y_{\leq n_Y} = A_{n_Y}^\top y \in \mathbb{R}^{n_Y}$, where A_{n_Y} and B_{n_Θ} are the matrices containing n_Y and n_Θ largest eigenvectors of H_Y and H_Θ , respectively. Realizations of posterior samples generated by the conditional DIRT for different observed data sets are presented in Appendix E.

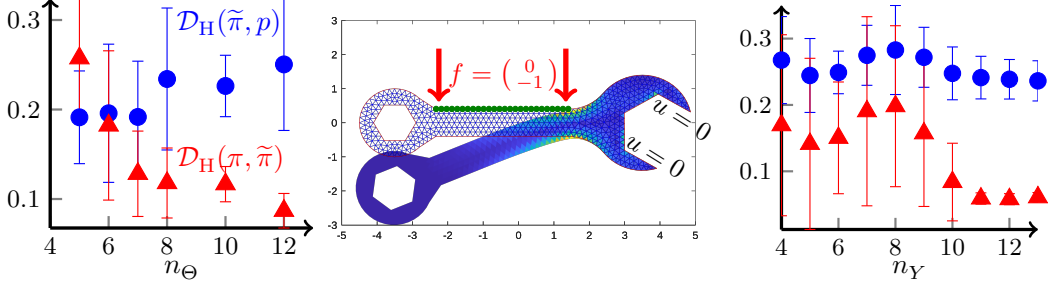


Figure 2: Wrench domain \mathcal{D} (middle), Hellinger distances (mean \pm std over 10 data samples) between DIRT approximation and reduced posterior, and between reduced and full posteriors with n_Θ varied and $n_Y = 13$ fixed (left), and n_Y varied and $n_\Theta = 13$ fixed (right).

The Hellinger distances between the DIRT approximation and the exact reduced-dimensional posterior, and the Hellinger distances between reduced and full posteriors are shown in Figure 2 (left and right). We fix the TT ranks to be 13 and specify tempering parameters $\beta_0 = 10^{-3}$, $\beta_{\ell+1} = \sqrt{10}\beta_\ell$. Further numerical tests on the DIRT error with varying TT rank and tempering step are shown in Appendix E. We observe that the DIRT accuracy degrades slowly with increasing dimension, since the TT decomposition needs to capture more correlations. However, higher dimensions deliver a more accurate parametrization of the random fields. A reasonable strategy is to choose the dimension such that the sum of two errors is minimal. In this example, this is achieved for $n_Y = 13$ and $n_\Theta = 7$.

Elliptic PDE with Besov prior. We consider the PDE $-\nabla(\kappa\nabla u) = f$ on $\mathcal{D} = [0, 1]^2$, in which the goal is to estimate the diffusion field $\kappa : \mathcal{D} \rightarrow \mathbb{R}_{>0}$ from partial observations of the potential function $u : \mathcal{D} \rightarrow \mathbb{R}$. We model the log of the diffusion field by a Besov- \mathcal{B}_{pp}^r prior [14, 29]. That is, given a wavelet basis $\{\psi_{j,k}^r\}$, where j controls the scaling, k controls the shift, and r controls the decay of the weighting coefficients, we have $\log \kappa = c_0 + \sum_{j=0}^J \sum_{k=0}^{2^j-1} b_{j,k} \psi_{j,k}^r$. This way, $\log \kappa$ is determined by the vector $\theta = (c_0, b_{0,0}, b_{0,1}, \dots) \in \mathbb{R}^{d_\Theta}$, $d_\Theta = 2^J + 1$, which is equipped with a product-form prior $\rho_\Theta(\theta) \propto \prod_{i=1}^{d_\Theta} \exp(-\gamma|\theta_i|^p)$. We choose $r = 2$ and $p = 1$ in this example, so effectively the parameter θ follows a Laplace prior. We order θ_i according to Proposition 1. The data are noisy observation of $u = u(\theta)$ evaluated at $d_Y = 16$ equispaced locations $\{s_i\}_{i=1}^{d_Y} \in \mathcal{D}$ perturbed by a centered Gaussian noise with the signal-to-noise-ratio 5.

Realizations of posterior samples generated by the conditional DIRT for different observed data sets are presented in Appendix E. Here we focus on demonstrating the accuracy of conditional DIRT. In Figure 3 (top), we let the TT-Cross approximation method truncate the TT ranks from the maximal values of 11 down to the minimal values that provide the relative maximum error below 0.1, and plot $\text{rank}_{\text{TT}}(\mathcal{T}_{\ell-1}^\# \pi_{Y,\Theta}^\ell)$ for each DIRT layer, as well as the average of TT ranks over ℓ . The tempering parameters are $\beta_0 = 10^{-4}$ and $\beta_{\ell+1} = \sqrt{10} \cdot \beta_\ell$. In the top left plot of Figure 3 we vary the order of variables, and in the top right plot we vary the number of θ_i variables from 12 to 22. We see that the order following Proposition 1 and Eq. (5) gives smallest TT ranks. Moreover, in this ordering, the intermediate TT ranks are independent of the total number of variables.

In Figure 3 (bottom) we compare the accuracy and complexity of the DIRT approximation in both the adaptive regime of TT ranks, and for fixed TT ranks, where the previous DIRT layer is used as the initial guess for the TT-Cross method on the next layer. The adaptive-rank results are shown as green lines (dashed for $n_\Theta = 12$, solid for $n_\Theta = 22$) spanning the TT ranks from 1 to 11. Fixed-rank results are shown as blue points at the corresponding rank values. Moreover, red baselines show the distance between the exact distributions in reduced and full spaces.

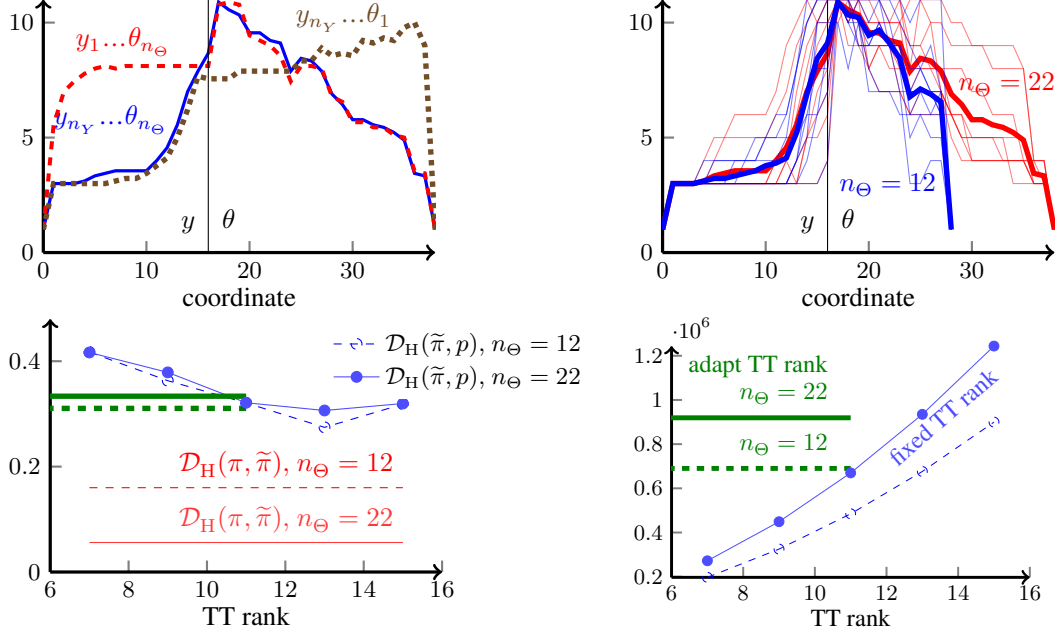


Figure 3: Besov prior example. Top: TT ranks of bridging densities approximated to inf-norm relative tolerance 10^{-1} . Left: average TT ranks over all DIRT layers for different orders of variables with $n_\Theta = 22$. Right: individual (thin) and average (thick) TT ranks over DIRT layers with $n_\Theta = 12$ and $n_\Theta = 22$ and the optimal variable order. Bottom Left: Hellinger-distance error between DIRT approximation and exact reduced posterior with $n_\Theta = 12$ and $n_\Theta = 22$, and between reduced and full posteriors. Bottom Right: Number of density evaluations in the construction of DIRT.

Again, the reduced dimensional joint density admits a more accurate DIRT approximation. This comes at a price of a larger distance towards the exact density in the original space, but that is still smaller than the DIRT error. The two strategies for the TT rank selection demonstrate comparable results by mutually compensating two aspects: the adaptive strategy allows one to reduce the ranks between the trailing variables, and hence the total number of function evaluations per one TT-Cross iteration, but several iterations carried out to reach the largest ranks inflate the number of evaluations.

This indicates that for lower-dimensional problems a simple fixed-rank DIRT might be more efficient, involving only an unsophisticated setup of the temperatures. For higher-dimensional problems one may prefer a rank-adaptive strategy to reduce the cost contributed by unimportant variables.

6 Conclusion

We develop a tensor approximation method to mitigate the computational burden of the characterization of conditional beliefs. This method employs the TT decomposition to approximate the joint pdf of the belief random variables and the observational random variables in the offline phase. The resulting conditional transport can rapidly characterize the conditional beliefs given new observed data in the online phase. Compared with most of the normalizing flows that can be viewed as density estimation, our method is based on function approximation. We exploit this function approximation perspective further to develop a new gradient-based technique to reorder and/or reparameterize the variables to enhance the approximation power of TT. We also integrate the TT-based transport maps and the parameter reordering/reparameterization into the layered structure of DIRT to further improve the performance of the resulting transport maps. We also provide error analysis to each element of our proposed computational framework. As shown in the SIR example, although DIRT is computationally more efficient than HINT in the offline phase and can be more accurate in the online phase, the major computational bottleneck of DIRT is that evaluating the map requires solving a sequence of root finding problems of monotone functions. Fortunately, this bottleneck can be alleviated by implementing DIRT on GPUs and parallel computing platforms.

A Proofs and derivations in Section 1

A.1 Useful lemmas

The following lemmas will be used to establish the probabilistic error bound of the conditional transport in (2).

Lemma 1. *Let π_1 and π_2 be two probability density functions such that $\mathcal{D}_H(\pi_1, \pi_2) \leq e < 1/\sqrt{2}$. For any function h with finite variances $\text{Var}_{\pi_1}(h) < \infty$ and $\text{Var}_{\pi_2}(h) < \infty$, the expectation error satisfies the following inequality*

$$|\mathbb{E}_{\pi_1}(h) - \mathbb{E}_{\pi_2}(h)| \leq \frac{\sqrt{2}e}{1 - \sqrt{2}e} \left(\sqrt{\text{Var}_{\pi_1}(h)} + \sqrt{\text{Var}_{\pi_2}(h)} \right).$$

Proof. Defining a function $\tilde{h}(x) := h(x) - \mathbb{E}_{\pi_1}(h)$, the mean squared error satisfies

$$\begin{aligned} |\mathbb{E}_{\pi_1}(h) - \mathbb{E}_{\pi_2}(h)| &= |\mathbb{E}_{\pi_1}(\tilde{h}) - \mathbb{E}_{\pi_2}(\tilde{h})| \\ &= \left| \int \tilde{h}(x) \left(\sqrt{\pi_1(x)} + \sqrt{\pi_2(x)} \right) \left(\sqrt{\pi_1(x)} - \sqrt{\pi_2(x)} \right) dx \right| \\ &\leq \left(\int \left(\sqrt{\pi_1(x)} - \sqrt{\pi_2(x)} \right)^2 dx \right)^{\frac{1}{2}} \left(\int \tilde{h}(x)^2 \left(\sqrt{\pi_1(x)} + \sqrt{\pi_2(x)} \right)^2 dx \right)^{\frac{1}{2}} \\ &= \sqrt{2} \mathcal{D}_H(\pi_1, \pi_2) \left(\int \left(\tilde{h}(x) \sqrt{\pi_1(x)} + \tilde{h}(x) \sqrt{\pi_2(x)} \right)^2 dx \right)^{\frac{1}{2}} \\ &\leq \sqrt{2} \mathcal{D}_H(\pi_1, \pi_2) \left(\left(\int (h(x) - \mathbb{E}_{\pi_1}(h))^2 \pi_1(x) dx \right)^{\frac{1}{2}} + \left(\int (h(x) - \mathbb{E}_{\pi_1}(h))^2 \pi_2(x) dx \right)^{\frac{1}{2}} \right) \\ &= \sqrt{2} \mathcal{D}_H(\pi_1, \pi_2) \left(\sqrt{\text{Var}_{\pi_1}(h)} + \left(\text{Var}_{\pi_2}(h) + |\mathbb{E}_{\pi_2}(h) - \mathbb{E}_{\pi_1}(h)|^2 \right)^{\frac{1}{2}} \right) \\ &\leq \sqrt{2} \mathcal{D}_H(\pi_1, \pi_2) \left(\sqrt{\text{Var}_{\pi_1}(h)} + \sqrt{\text{Var}_{\pi_2}(h)} + |\mathbb{E}_{\pi_1}(h) - \mathbb{E}_{\pi_2}(h)| \right) \end{aligned}$$

Substituting the condition $\mathcal{D}_H(\pi_1, \pi_2) \leq e$, we obtain

$$(1 - \sqrt{2}e) |\mathbb{E}_{\pi_1}(h) - \mathbb{E}_{\pi_2}(h)| \leq \sqrt{2}e \left(\sqrt{\text{Var}_{\pi_1}(h)} + \sqrt{\text{Var}_{\pi_2}(h)} \right),$$

and, because $\sqrt{2}e < 1$, the result follows. \square

Lemma 2. *For two joint pdfs $\pi_{Y,\Theta}$ and $\tilde{\pi}_{Y,\Theta}$ and a given realization y , the expected Hellinger distance between $\pi_{\Theta|Y}$ and $\tilde{\pi}_{\Theta|Y}$ satisfies*

$$\mathbb{E}_{Y \sim \pi_Y} [\mathcal{D}_H(\pi_{\Theta|Y}, \tilde{\pi}_{\Theta|Y})] \leq 2\mathcal{D}_H(\pi_{Y,\Theta}, \tilde{\pi}_{Y,\Theta}).$$

Proof. Applying Jensen's inequality, we have

$$\mathbb{E}_{Y \sim \pi_Y} [\mathcal{D}_H(\pi_{\Theta|Y}, \tilde{\pi}_{\Theta|Y})] \leq \sqrt{\mathbb{E}_{Y \sim \pi_Y} [\mathcal{D}_H(\pi_{\Theta|Y}, \tilde{\pi}_{\Theta|Y})^2]}.$$

The expected squared Hellinger distance between $\pi_{\Theta|Y}$ and $\tilde{\pi}_{\Theta|Y}$ satisfies

$$\begin{aligned} &\mathbb{E}_{Y \sim \pi_Y} [\mathcal{D}_H(\pi_{\Theta|Y}, \tilde{\pi}_{\Theta|Y})^2] \\ &= \int \left(\frac{1}{2} \int \left(\sqrt{\pi_{\Theta|Y}(\theta|y)} - \sqrt{\tilde{\pi}_{\Theta|Y}(\theta|y)} \right)^2 d\theta \right) \pi_Y(y) dy \\ &= \frac{1}{2} \int \left(\sqrt{\pi_{Y,\Theta}(y, \theta)} - \sqrt{\tilde{\pi}_{Y,\Theta}(y, \theta)} \frac{\pi_Y(y)}{\tilde{\pi}_Y(y)} \right)^2 d\theta dy \\ &\leq \int \left(\sqrt{\pi_{Y,\Theta}(y, \theta)} - \sqrt{\tilde{\pi}_{Y,\Theta}(y, \theta)} \right)^2 d\theta dy + \int \left(\sqrt{\tilde{\pi}_{Y,\Theta}(y, \theta)} - \sqrt{\tilde{\pi}_{Y,\Theta}(y, \theta)} \frac{\pi_Y(y)}{\tilde{\pi}_Y(y)} \right)^2 d\theta dy \end{aligned}$$

$$\begin{aligned}
&= 2\mathcal{D}_H(\pi_{Y,\Theta}, \tilde{\pi}_{Y,\Theta})^2 + \int \left(\sqrt{\tilde{\pi}_Y(y)} - \sqrt{\pi_Y(y)} \right)^2 dy \\
&= 2\mathcal{D}_H(\pi_{Y,\Theta}, \tilde{\pi}_{Y,\Theta})^2 + 2\mathcal{D}_H(\pi_Y, \tilde{\pi}_Y)^2.
\end{aligned}$$

The squared Hellinger distance between the marginal pdfs satisfies

$$\begin{aligned}
\mathcal{D}_H(\pi_Y, \tilde{\pi}_Y)^2 &= \frac{1}{2} \int \left(\sqrt{\frac{\tilde{\pi}_Y(y)}{\pi_Y(y)}} - 1 \right)^2 \pi_Y(y) dy \\
&= \frac{1}{2} \int \left(\sqrt{\int \frac{\tilde{\pi}_{Y,\Theta}(y, \theta)}{\pi_{Y,\Theta}(y, \theta)} \pi_{\Theta|Y}(\theta|y) d\theta} - \sqrt{\int \pi_{\Theta|Y}(\theta|y) d\theta} \right)^2 \pi_Y(y) dy \\
&\leq \frac{1}{2} \int \left(\int \left(\sqrt{\frac{\tilde{\pi}_{Y,\Theta}(y, \theta)}{\pi_{Y,\Theta}(y, \theta)}} - 1 \right)^2 \pi_{\Theta|Y}(\theta|y) d\theta \right) \pi_Y(y) dy \\
&= \frac{1}{2} \int \left(\sqrt{\frac{\tilde{\pi}_{Y,\Theta}(y, \theta)}{\pi_{Y,\Theta}(y, \theta)}} - 1 \right)^2 \pi_{Y,\Theta}(y, \theta) d\theta dy \\
&= \mathcal{D}_H(\pi_{Y,\Theta}, \tilde{\pi}_{Y,\Theta})^2,
\end{aligned}$$

where the inequality follows from Jensen's inequality. This way, we have

$$\mathbb{E}_{Y \sim \pi_Y} [\mathcal{D}_H(\pi_{\Theta|Y}, \tilde{\pi}_{\Theta|Y})^2] \leq 4\mathcal{D}_H(\pi_{Y,\Theta}, \tilde{\pi}_{Y,\Theta})^2,$$

and thus the result follows. \square

A.2 A probabilistic error bound of the conditional transport

Suppose the Hellinger distance between the joint pdfs $\pi_{Y,\Theta}$ and $\tilde{\pi}_{Y,\Theta}$ satisfies $\mathcal{D}_H(\pi_{Y,\Theta}, \tilde{\pi}_{Y,\Theta}) \leq \varepsilon$ for some $\varepsilon < \sqrt{2}/4$. For any $\tau \in [0, 1]$, applying Markov's inequality and Lemma 2 yields

$$\begin{aligned}
\mathbb{P}_{Y \sim \pi_Y} [\mathcal{D}_H(\pi_{\Theta|Y}, \tilde{\pi}_{\Theta|Y}) \leq \tau] &= 1 - \mathbb{P}_{Y \sim \pi_Y} [\mathcal{D}_H(\pi_{\Theta|Y}, \tilde{\pi}_{\Theta|Y}) > \tau] \\
&> 1 - \frac{\mathbb{E}_{Y \sim \pi_Y} [\mathcal{D}_H(\pi_{\Theta|Y}, \tilde{\pi}_{\Theta|Y})]}{\tau} \\
&\geq 1 - \frac{2\mathcal{D}_H(\pi_{Y,\Theta}, \tilde{\pi}_{Y,\Theta})}{\tau} \geq 1 - \frac{2\varepsilon}{\tau}.
\end{aligned}$$

Let $\delta = 2\varepsilon/\tau$, we deduce that $\mathcal{D}_H(\pi_{\Theta|Y}, \tilde{\pi}_{\Theta|Y}) \leq 2\varepsilon/\delta$ holds with probability greater than $1 - \delta$. Applying Lemma 1, with probability greater than $1 - \delta$, we have the event

$$\frac{|\mathbb{E}_{\pi_{\Theta|Y}}(h) - \mathbb{E}_{\tilde{\pi}_{\Theta|Y}}(h)|}{\sqrt{\text{Var}_{\pi_{\Theta|Y}}(h) + \text{Var}_{\tilde{\pi}_{\Theta|Y}}(h)}} \leq \frac{2\sqrt{2}\varepsilon/\delta}{1 - 2\sqrt{2}\varepsilon/\delta} = \frac{4\varepsilon}{\sqrt{2}\delta - 4\varepsilon}.$$

This concludes the result. \square

B Proofs and derivations in Section 2

B.1 SIRT error

Suppose we have an approximation g to $\sqrt{\pi_{Y,\Theta}}$ such that the L^2 error satisfies $\|\sqrt{\pi_{Y,\Theta}} - g\|_2 \leq \varepsilon/\sqrt{2}$. Let $z = \|g\|_2^2$ denote the normalizing constant of the approximate pdf $p_{Y,\Theta}(y, \theta) = \frac{1}{z}g(y, \theta)^2$. Then, the normalizing constant satisfies

$$\begin{aligned}
|z - 1| &= \left| \int (g^2 - \pi_{Y,\Theta}) dy d\theta \right| \\
&= \left| \int (g - \sqrt{\pi_{Y,\Theta}})(g + \sqrt{\pi_{Y,\Theta}}) dy d\theta \right|
\end{aligned}$$

$$\begin{aligned}
&\leq \left(\int (g - \sqrt{\pi_{Y,\Theta}})^2 dy d\theta \right)^{\frac{1}{2}} \left(\int (g + \sqrt{\pi_{Y,\Theta}})^2 dy d\theta \right)^{\frac{1}{2}} \\
&\leq \|\sqrt{\pi_{Y,\Theta}} - g\|_2 (\|g\|_2 + \|\sqrt{\pi_{Y,\Theta}}\|_2) \\
&= \|\sqrt{\pi_{Y,\Theta}} - g\|_2 (\sqrt{z} + 1).
\end{aligned}$$

Since $|z - 1| = |\sqrt{z} - 1|(\sqrt{z} + 1)$, the above inequality leads to $|\sqrt{z} - 1| \leq \|\sqrt{\pi_{Y,\Theta}} - g\|_2$. Next, we write

$$\begin{aligned}
\mathcal{D}_H(\pi_{Y,\Theta}, p_{Y,\Theta}) &= \frac{1}{\sqrt{2}} \left(\int (\sqrt{\pi_{Y,\Theta}} - \sqrt{p_{Y,\Theta}})^2 dy d\theta \right)^{\frac{1}{2}} \\
&= \frac{1}{\sqrt{2}} \left(\int \left(\sqrt{\pi_{Y,\Theta}} - g + g - \frac{1}{\sqrt{z}}g \right)^2 dy d\theta \right)^{\frac{1}{2}} \\
&\leq \frac{1}{\sqrt{2}} \left(\int (\sqrt{\pi_{Y,\Theta}} - g)^2 dy d\theta \right)^{\frac{1}{2}} + \frac{1}{\sqrt{2}} \left(\int g^2 \left(1 - \frac{1}{\sqrt{z}}\right)^2 dy d\theta \right)^{\frac{1}{2}} \\
&= \frac{1}{\sqrt{2}} \|\sqrt{\pi_{Y,\Theta}} - g\|_2 + \frac{|\sqrt{z} - 1|}{\sqrt{2}} \\
&\leq \sqrt{2} \|\sqrt{\pi_{Y,\Theta}} - g\|_2 \leq \varepsilon,
\end{aligned}$$

where we used $|\sqrt{z} - 1| \leq \|\sqrt{\pi_{Y,\Theta}} - g\|_2$ in the last inequality. This concludes the result. \square

B.2 Marginalizing squared TT factorization

Recall that we approximate the function $\sqrt{\pi_{Y,\Theta}}$ using a TT decomposition

$$g(y, \theta) = \mathcal{G}_{-d_Y}(y_{d_Y}) \dots \mathcal{G}_{-1}(y_1) \mathcal{G}_1(\theta_1) \dots \mathcal{G}_{d_\Theta}(\theta_{d_\Theta}).$$

In this subsection, we group the variables y and θ together for brevity. This way, we have the variable $x = (y, \theta) \in \mathbb{R}^d$, where $d = d_Y + d_\Theta$, can equivalently express the TT decomposition as

$$g(y, \theta) \equiv g(x) = \mathcal{G}_1(x_1) \dots \mathcal{G}_k(x_k) \dots \mathcal{G}_d(x_d),$$

where $\text{rank}_{\text{TT}}(g) = (r_0, \dots, r_k, \dots, r_d)$ gives the TT ranks of $g(x)$ with $r_0 = r_d = 1$. Using the function $g(x)$, one can approximate the target pdf $\pi(x) \equiv \pi_{Y,\Theta}(y, \theta)$ by

$$p(x) = \frac{1}{z_p} g(x)^2, \quad z_p = \int g(x)^2 dx. \quad (22)$$

Utilizing the separation of variables of the TT decomposition, the goal of this subsection is to derive the **marginal pdfs** of $p(x)$, denoted by

$$p_{\leq k}(x_{\leq k}) = \int p(x) dx_{k+1} \dots dx_d, \quad (23)$$

for $k = 1, 2, \dots, d-1$ and the normalizing constant z_p . Note that we have $p_{\leq d}(x_{\leq d}) \equiv p(x)$. This leads to the conditional pdfs

$$p_{X_k|X_{<k}}(x_k|x_{<k}) = \frac{p_{\leq k}(x_{\leq k})}{p_{<k}(x_{<k})}, \quad k = 2, \dots, d,$$

which are the key elements for defining the Rosenblatt transport in (8) in Section 2.

We represent each TT core of the decomposition by

$$\mathcal{G}_k^{(\alpha_{k-1}, \alpha_k)}(x_k) = \sum_{i=1}^{n_k} \phi_k^{(i)}(x_k) \mathcal{A}_k[\alpha_{k-1}, i, \alpha_k], \quad \alpha_{k-1} = 1, \dots, r_{k-1}, \quad \alpha_k = 1, \dots, r_k, \quad (24)$$

where $\{\phi_k^{(i)}(x_k)\}_{i=1}^{n_k}$ are the basis functions for the k -th coordinate and $\mathcal{A}_k \in \mathbb{R}^{r_{k-1} \times n_k \times r_k}$ is the associated k -th coefficient tensor. Then, applying Proposition 2 of [11], the marginal functions can be expressed as

$$p_1(x_1) = \sum_{\ell_1=1}^{r_1} \left(\mathcal{L}_1^{(\alpha_0, \ell_1)}(x_1) \right)^2, \quad (25)$$

$$p_{\leq k}(x_{\leq k}) = \sum_{\ell_k=1}^{r_k} \left(\mathcal{G}_{<k}^{(\alpha_{k-1})}(x_{<k}) \mathcal{L}_k^{(\alpha_{k-1}, \ell_k)}(x_k) \right)^2, \quad k = 2, \dots, d, \quad (26)$$

where $\alpha_0 = 1$ and

$$\mathcal{G}_{<k}^{(\alpha_{k-1})}(x_{<k}) = \mathcal{G}_1(x_1) \cdots \mathcal{G}_{k-1}^{(\cdot, \alpha_{k-1})}(x_{k-1}) : \mathcal{X}_{<k} \mapsto \mathbb{R}, \quad (27)$$

$$\mathcal{L}_k^{(\alpha_{k-1}, \ell_k)}(x_k) = \sum_{i=1}^{n_k} \phi_k^{(i)}(x_k) \mathbf{B}_k[\alpha_{k-1}, i, \ell_k] : \mathcal{X}_k \mapsto \mathbb{R}, \quad (28)$$

for a coefficient tensor $\mathbf{B}_k \in \mathbb{R}^{r_{k-1} \times n_k \times r_k}$ that is recursively defined in Algorithm 3.

Algorithm 3 Computing \mathcal{B} and z

For the k -th set of basis functions, we define the mass matrix $\mathbf{M}_k \in \mathbb{R}^{n_k \times n_k}$ by

$$\mathbf{M}_k[i, j] = \int_{\mathcal{X}_k} \phi_k^{(i)}(x_k) \phi_k^{(j)}(x_k) dx_k, \quad \text{for } i = 1, \dots, n_k, j = 1, \dots, n_k. \quad (29)$$

Starting with the last coordinate $k = d$, we set $\mathbf{B}_d = \mathcal{A}_d$. Suppose for the first k dimensions ($k > 1$), we have a coefficient tensor $\mathbf{B}_k \in \mathbb{R}^{r_{k-1} \times n_k \times r_k}$ that defines a marginal function $p_{\leq k}(x_{\leq k})$ as in (26). The following procedure can be used to obtain the coefficient tensor $\mathbf{B}_{k-1} \in \mathbb{R}^{r_{k-2} \times n_{k-1} \times r_{k-1}}$ for defining the next marginal function $p_{<k}(x_{<k})$:

1. Use the Cholesky factorisation of the mass matrix, $\mathbf{L}_k \mathbf{L}_k^\top = \mathbf{M}_k \in \mathbb{R}^{n_k \times n_k}$, to construct a tensor $\mathcal{C}_k \in \mathbb{R}^{r_{k-1} \times n_k \times r_k}$:

$$\mathcal{C}_k[\alpha_{k-1}, \tau, \ell_k] = \sum_{i=1}^{n_k} \mathbf{B}_k[\alpha_{k-1}, i, \ell_k] \mathbf{L}_k[i, \tau]. \quad (30)$$

2. Unfold \mathcal{C}_k along the first coordinate [25] to obtain a matrix $\mathbf{C}_k^{(R)} \in \mathbb{R}^{r_{k-1} \times (n_k r_k)}$ and compute the thin QR factorisation

$$\mathbf{Q}_k \mathbf{R}_k = (\mathbf{C}_k^{(R)})^\top, \quad (31)$$

where $\mathbf{Q}_k \in \mathbb{R}^{(n_k r_k) \times r_{k-1}}$ is semi-orthogonal and $\mathbf{R}_k \in \mathbb{R}^{r_{k-1} \times r_{k-1}}$ is upper-triangular.

3. Compute the new coefficient tensor

$$\mathbf{B}_{k-1}[\alpha_{k-2}, i, \ell_{k-1}] = \sum_{\alpha_{k-1}=1}^{r_{k-1}} \mathcal{A}_{k-1}[\alpha_{k-2}, i, \alpha_{k-1}] \mathbf{R}_k[\ell_{k-1}, \alpha_{k-1}]. \quad (32)$$

Furthermore, at index $k = 1$, the unfolded \mathcal{C}_1 along the first coordinate is a row vector $\mathbf{C}_1^{(R)} \in \mathbb{R}^{1 \times (n_1 r_1)}$. Thus, the thin QR factorisation $\mathbf{Q}_1 \mathbf{R}_1 = (\mathbf{C}_1^{(R)})^\top$ produces a scalar $\mathbf{R}_1 \in \mathbb{R}$ and the normalising constant $z_p = \int_{\mathcal{X}_1} p_{\leq 1}(x_1) dx_1$ can be obtained by $z_p = \mathbf{R}_1^2 = \|\mathbf{C}_1^{(R)}\|^2$.

C Proofs and derivations in Section 3

C.1 Coordinate selection driven by the Poincaré inequality

The results in Section 3 rely on the following lemma.

Lemma 3. *Let $\rho(x) = \rho_1(x_1) \cdots \rho_d(x_d)$ be a product-form pdf on \mathbb{R}^d that satisfies the Poincaré inequality, that is, there exists a constant $\kappa < \infty$ such that*

$$\int \left(h(x) - \int h(x) \rho(x) dx \right)^2 \rho(x) dx \leq \kappa \int \|\nabla h(x)\|^2 \rho(x) dx, \quad (33)$$

holds for any sufficiently smooth function $h : \mathbb{R}^d \rightarrow \mathbb{R}$, where $\|\cdot\|$ denotes the euclidean norm. Let π be a pdf on \mathbb{R}^d . Given $n < d$, consider the pdf $\tilde{\pi}^*$ on \mathbb{R}^d defined by $\tilde{\pi}^*(x) \propto g(x_{\leq n})^2 \rho(x)$ where $g : \mathbb{R}^n \rightarrow \mathbb{R}_{\geq 0}$ is defined by

$$g(x_{\leq n}) = \int \left(\frac{\pi(x_{\leq n}, x_{>n})}{\rho(x_{\leq n}, x_{>n})} \right)^{\frac{1}{2}} \rho_{>n}(x_{>n}) dx_{>n}. \quad (34)$$

Then we have

$$\mathcal{D}_H(\pi, \tilde{\pi}^*)^2 \leq \frac{\kappa}{4} \sum_{i=n+1}^d H_{ii}, \quad (35)$$

where $H = \int (\nabla \log \frac{\pi(x)}{\rho(x)}) (\nabla \log \frac{\pi(x)}{\rho(x)})^\top \pi(x) dx$.

Proof. We denote the norm and the scalar product of $L^2 := \{u : \mathbb{R}^d \rightarrow \mathbb{R} : \int u^2 dx < \infty\}$ by $\|\cdot\|$ and $\langle \cdot, \cdot \rangle$, respectively. Letting $f(x) = g(x_{\leq n}) \sqrt{\rho(x)}$, we have the identity

$$\begin{aligned} \langle f, \sqrt{\pi} \rangle &= \int g(x_{\leq n}) \sqrt{\pi(x)/\rho(x)} \rho(x) dx \\ &= \int g(x_{\leq n}) \underbrace{\left(\int \left(\frac{\pi(x_{\leq n}, x_{>n})}{\rho(x_{\leq n}, x_{>n})} \right)^{\frac{1}{2}} \rho_{>n}(x_{>n}) dx_{>n} \right)}_{=g(x_{\leq n})} \rho_{\leq n}(x_{\leq n}) dx_{\leq n} \\ &= \int g(x_{\leq n})^2 \rho(x) dx = \|f\|^2. \end{aligned} \quad (36)$$

Furthermore, $\tilde{\pi}^*(x) \propto g(x_{\leq n})^2 \rho(x) = f(x)^2$ writes $\tilde{\pi}^*(x) = \frac{f(x)^2}{\|f\|^2}$ and satisfies

$$\mathcal{D}_H(\pi, \tilde{\pi}^*)^2 = \frac{1}{2} \left\| \sqrt{\pi} - \frac{f}{\|f\|} \right\|^2 = 1 - \left\langle \sqrt{\pi}, \frac{f}{\|f\|} \right\rangle \stackrel{(36)}{=} 1 - \|f\|. \quad (37)$$

Because $\mathcal{D}_H(\pi, \tilde{\pi}^*)^2 \geq 0$, we have $0 \leq \|f\| \leq 1$ so that

$$1 - \|f\| \leq 1 - \|f\|^2 \stackrel{(36)}{=} \|\sqrt{\pi} - f\|^2.$$

Thus, we have $\mathcal{D}_H(\pi, \tilde{\pi}^*)^2 \leq \|\sqrt{\pi} - f\|^2$. Letting $h(x) = \sqrt{\pi(x)/\rho(x)}$, we obtain

$$\begin{aligned} \mathcal{D}_H(\pi, \tilde{\pi}^*)^2 &\leq \int \left(\sqrt{\pi(x)} - f(x) \right)^2 dx = \int \left(h(x) - g(x_{\leq n}) \right)^2 \rho(x) dx \\ &\stackrel{(34)}{=} \int \left(\int \left(h(x_{\leq n}, x_{>n}) - \int h(x_{\leq n}, x'_{>n}) \rho_{>n}(x'_{>n}) dx'_{>n} \right)^2 \rho_{>n}(x_{>n}) dx_{>n} \right) \rho_{\leq n}(x_{\leq n}) dx_{\leq n} \\ &\leq \kappa \int \|\nabla_{>n} h(x_{\leq n}, x_{>n})\|_2^2 \rho(x) dx = \kappa \sum_{i=n+1}^d \int (\partial_i h(x))^2 \rho(x) dx. \end{aligned} \quad (38)$$

The previous inequality (38) is obtained by applying the Poincaré inequality (33) to the function $h_{>n} : x_{>n} \mapsto h(x_{\leq n}, x_{>n})$. To conclude the proof, it remains to show that $\int (\partial_i h(x))^2 \rho(x) dx = \frac{1}{4} H_{ii}$, which can be given as follows

$$\begin{aligned} \int (\partial_i h(x))^2 \rho(x) dx &= \int \left(\partial_i \sqrt{\pi(x)/\rho(x)} \right)^2 \rho(x) dx \\ &= \frac{1}{4} \int \left(\frac{\partial_i (\pi(x)/\rho(x))}{\sqrt{\pi(x)/\rho(x)}} \right)^2 \rho(x) dx \\ &= \frac{1}{4} \int \left(\sqrt{\pi(x)/\rho(x)} \partial_i \log \left(\pi(x)/\rho(x) \right) \right)^2 \rho(x) dx \\ &= \frac{1}{4} \int \left(\partial_i \log \left(\pi(x)/\rho(x) \right) \right)^2 \pi(x) dx = \frac{1}{4} H_{ii}. \end{aligned}$$

This concludes the proof. \square

C.2 Proof of Proposition 1

Proposition 1 can be shown by applying Lemma 3 with

$$\begin{aligned} x &= (y, \theta) \in \mathbb{R}^d, \\ d &= d_Y + d_\Theta, \\ n &= n_Y + n_\Theta, \\ x_{\leq n} &= (y_1, \dots, y_{n_Y}, \theta_1, \dots, \theta_{n_\Theta}) \in \mathbb{R}^n, \\ x_{>n} &= (y_{n_Y+1}, \dots, y_{d_Y}, \theta_{n_\Theta+1}, \dots, \theta_{d_\Theta}) \in \mathbb{R}^{d-n}, \\ \pi(x) &= \pi_{Y,\Theta}(y, \theta), \\ \rho(x) &= \rho_{Y,\Theta}(y, \theta). \end{aligned}$$

With these notations, Lemma 3 ensures the existence of a pdf of the form of

$$\tilde{\pi}_{Y,\Theta}(y, \theta) \propto g(y_{\leq n_Y}, \theta_{\leq n_\Theta})^2 \rho_{Y,\Theta}(y, \theta)$$

with

$$g(y_{\leq n_\Theta}, \theta_{\leq n_\Theta}) \stackrel{(34)}{=} \int \left(\frac{\pi_{Y,\Theta}(y, \theta)}{\rho_{Y,\Theta}(y, \theta)} \right)^{\frac{1}{2}} \rho_{Y_{>n_Y}, \Theta_{>n_\Theta}}(y_{>n_Y}, \theta_{>n_\Theta}) dy_{>n_Y} d\theta_{>n_\Theta},$$

such that

$$\mathcal{D}_H(\pi_{Y,\Theta}, \tilde{\pi}_{Y,\Theta})^2 \stackrel{(35)}{\leq} \frac{\kappa}{4} \left(\sum_{i=n_Y+1}^{d_Y} (H_Y)_{ii} + \sum_{j=n_\Theta+1}^{d_\Theta} (H_\Theta)_{jj} \right).$$

The pdf $\tilde{\pi}_{Y,\Theta}(y, \theta)$ can be equivalently written as

$$\tilde{\pi}_{Y,\Theta}(y, \theta) = \left(\prod_{i=n_Y+1}^{d_Y} \rho_{Y_i}(y_i) \right) \tilde{\pi}_{Y_{\leq n_Y}, \Theta_{\leq n_\Theta}}(y_{\leq n_\Theta}, \theta_{\leq n_\Theta}) \left(\prod_{j=n_\Theta+1}^{d_\Theta} \rho_{\Theta_j}(\theta_j) \right),$$

with

$$\tilde{\pi}_{Y_{\leq n_Y}, \Theta_{\leq n_\Theta}}(y_{\leq n_\Theta}, \theta_{\leq n_\Theta}) \propto g(y_{\leq n_\Theta}, \theta_{\leq n_\Theta}) \left(\prod_{i=1}^{n_Y} \rho_{Y_i}(y_i) \right) \left(\prod_{j=1}^{n_\Theta} \rho_{\Theta_j}(\theta_j) \right).$$

This concludes the proof. \square

C.3 Optimality of the approximate pdf

Lemma 3 shows that there exists an approximate pdf $\tilde{\pi}^*(x) \propto g(x_{\leq n})^2 \rho(x)$ with g as in (34) such that the inequality (35) holds. In fact, among all densities of the form $\tilde{\pi}(x) \propto \tilde{g}(x_{\leq n})^2 \rho(x)$ for some function $\tilde{g} : \mathbb{R}^n \rightarrow \mathbb{R}$, the choice (34) is optimal in the sense that it minimizes the Hellinger distance $\mathcal{D}_H(\pi, \tilde{\pi})$. This result is given by the following lemma, which does not require the product-form of ρ .

Lemma 4. *Let π and ρ be two pdfs on \mathbb{R}^d . For any $n < d$, let $\tilde{\pi}^*$ be the pdf on \mathbb{R}^d defined by $\tilde{\pi}^*(x) \propto g(x_{\leq n})^2 \rho(x)$, where $g : \mathbb{R}^n \rightarrow \mathbb{R}_{\geq 0}$ is defined by*

$$g(x_{\leq n}) = \int \left(\frac{\pi(x_{\leq n}, x_{>n})}{\rho(x_{\leq n}, x_{>n})} \right)^{\frac{1}{2}} \rho_{>n|\leq n}(x_{>n}|x_{\leq n}) dx_{>n}. \quad (39)$$

Here, $\rho_{>n|\leq n}(x_{>n}|x_{\leq n}) = \rho(x_{\leq n}, x_{>n}) / \rho_{\leq n}(x_{\leq n})$ is a conditional pdf. For any function $\tilde{g} : \mathbb{R}^n \rightarrow \mathbb{R}_{\geq 0}$ such that $\tilde{\pi} \propto \tilde{g}(x_{\leq n})^2 \rho(x)$ is a pdf, we have

$$\mathcal{D}_H(\pi, \tilde{\pi})^2 = \mathcal{D}_H(\pi, \tilde{\pi}^*)^2 + \|g\sqrt{\rho(x)}\| \mathcal{D}_H(\tilde{\pi}^*, \tilde{\pi})^2. \quad (40)$$

In particular $\mathcal{D}_H(\pi, \tilde{\pi}^) \leq \mathcal{D}_H(\pi, \tilde{\pi})$ holds for any \tilde{g} and equality is attained when $\mathcal{D}_H(\tilde{\pi}^*, \tilde{\pi}) = 0$, meaning that $\tilde{g} = g$ in the L^2 -sense.*

Proof. We denote the norm and the scalar product of $L^2 := \{u : \mathbb{R}^d \rightarrow \mathbb{R} : \int u^2 dx < \infty\}$ by $\|\cdot\|$ and $\langle \cdot, \cdot \rangle$, respectively. Let $\tilde{f}(x) = \tilde{g}(x_{\leq n})\sqrt{\rho(x)}$ and $f(x) = g(x_{\leq n})\sqrt{\rho(x)}$. We have

$$\begin{aligned} \langle \tilde{f}, \sqrt{\pi} \rangle &= \int \tilde{g}(x_{\leq n})\sqrt{\pi(x)/\rho(x)}\rho(x)dx \\ &= \int \tilde{g}(x_{\leq n}) \underbrace{\left(\int \left(\frac{\pi(x_{\leq n}, x_{>n})}{\rho(x_{\leq n}, x_{>n})} \right)^{\frac{1}{2}} \rho_{>n|\leq n}(x_{>n}|x_{\leq n})dx_{>n} \right)}_{=g(x_{\leq n})} \rho_{\leq n}(x_{\leq n})dx_{\leq n} \\ &= \int \tilde{g}(x_{\leq n})g(x_{\leq n})\rho(x)dx = \langle \tilde{f}, f \rangle. \end{aligned} \quad (41)$$

Similarly we have $\langle f, \sqrt{\pi} \rangle = \langle f, f \rangle$. This yields

$$\begin{aligned} \mathcal{D}_{\text{H}}(\pi, \tilde{\pi})^2 &= \frac{1}{2} \left\| \left(\sqrt{\pi} - \frac{f}{\|f\|} \right) + \left(\frac{f}{\|f\|} - \frac{\tilde{f}}{\|\tilde{f}\|} \right) \right\|^2 \\ &= \mathcal{D}_{\text{H}}(\pi, \tilde{\pi}^*)^2 + \left\langle \sqrt{\pi} - \frac{f}{\|f\|}, \frac{f}{\|f\|} - \frac{\tilde{f}}{\|\tilde{f}\|} \right\rangle + \mathcal{D}_{\text{H}}(\tilde{\pi}^*, \tilde{\pi})^2 \\ &\stackrel{(41)}{=} \mathcal{D}_{\text{H}}(\pi, \tilde{\pi}^*)^2 + \left\langle f - \frac{f}{\|f\|}, \frac{f}{\|f\|} - \frac{\tilde{f}}{\|\tilde{f}\|} \right\rangle + \mathcal{D}_{\text{H}}(\tilde{\pi}^*, \tilde{\pi})^2 \\ &= \mathcal{D}_{\text{H}}(\pi, \tilde{\pi}^*)^2 + (\|f\| - 1) \left(1 - \frac{\langle f, \tilde{f} \rangle}{\|f\|\|\tilde{f}\|} \right) + \mathcal{D}_{\text{H}}(\tilde{\pi}^*, \tilde{\pi})^2 \\ &= \mathcal{D}_{\text{H}}(\pi, \tilde{\pi}^*)^2 + (\|f\| - 1) \mathcal{D}_{\text{H}}(\tilde{\pi}^*, \tilde{\pi})^2 + \mathcal{D}_{\text{H}}(\tilde{\pi}^*, \tilde{\pi})^2 \\ &= \mathcal{D}_{\text{H}}(\pi, \tilde{\pi}^*)^2 + \|f\| \mathcal{D}_{\text{H}}(\tilde{\pi}^*, \tilde{\pi})^2, \end{aligned}$$

and thus the results follow. \square

C.4 Proof of Proposition 2

Proposition 2 can be shown by applying Proposition 1 after a reparametrization. Let $A \in \mathbb{R}^{d_Y \times d_Y}$ and $B \in \mathbb{R}^{d_{\Theta} \times d_{\Theta}}$ be a pair of unitary matrices and consider the change of variable

$$\bar{y} = A^{\top} y \quad \text{and} \quad \bar{\theta} = B^{\top} \theta.$$

Because $\rho_{Y, \Theta}$ is Gaussian with identity covariance, for $(U_{\Theta}, U_Y) \sim \rho_{Y, \Theta}$, the reparametrized random variable $(A^{\top} U_Y, B^{\top} U_{\Theta})$ is also Gaussian with identity covariance. Since any Gaussian pdf with identity covariance matrix satisfies Poincaré inequality with $\kappa = 1$, see [8], Proposition 1 ensures there exists a pdf $\tilde{\pi}_{\bar{Y}, \bar{\Theta}}(\bar{y}, \bar{\theta})$ as in (9) such that

$$\mathcal{D}_{\text{H}}(\pi_{\bar{Y}, \bar{\Theta}}, \tilde{\pi}_{\bar{Y}, \bar{\Theta}})^2 \leq \frac{1}{4} \left(\sum_{i=n_Y+1}^{d_Y} (H_Y^A)_{ii} + \sum_{j=n_{\Theta}+1}^{d_{\Theta}} (H_{\Theta}^B)_{jj} \right), \quad (42)$$

where $\pi_{\bar{Y}, \bar{\Theta}}$ is the pdf of $(A^{\top} Y, B^{\top} \Theta)$ and where H_Y^A and H_{Θ}^B are given by

$$\begin{aligned} H_Y^A &= \int \left(\nabla_y \log \frac{\pi_{\bar{Y}, \bar{\Theta}}}{\rho_{\bar{Y}, \bar{\Theta}}} \right) \left(\nabla_y \log \frac{\pi_{\bar{Y}, \bar{\Theta}}}{\rho_{\bar{Y}, \bar{\Theta}}} \right)^{\top} d\pi_{\bar{Y}, \bar{\Theta}}, \\ H_{\Theta}^B &= \int \left(\nabla_{\theta} \log \frac{\pi_{\bar{Y}, \bar{\Theta}}}{\rho_{\bar{Y}, \bar{\Theta}}} \right) \left(\nabla_{\theta} \log \frac{\pi_{\bar{Y}, \bar{\Theta}}}{\rho_{\bar{Y}, \bar{\Theta}}} \right)^{\top} d\pi_{\bar{Y}, \bar{\Theta}}. \end{aligned}$$

Applying the chain rule, we have $H_Y^A = A^{\top} H_Y A$ and $H_{\Theta}^B = B^{\top} H_{\Theta} B$. Thus, defining A and B as the matrices containing the eigenvectors (with corresponding eigenvalues sorted in the decreasing order) of H_Y and H_{Θ} respectively, the inequality in (42) becomes

$$\mathcal{D}_{\text{H}}(\pi_{\bar{Y}, \bar{\Theta}}, \tilde{\pi}_{\bar{Y}, \bar{\Theta}})^2 \leq \frac{1}{4} \left(\sum_{i=n_Y+1}^{d_Y} \lambda_i(H_Y) + \sum_{j=n_{\Theta}+1}^{d_{\Theta}} \lambda_j(H_{\Theta}) \right),$$

where $\lambda_i(\cdot)$ denotes the i -th largest eigenvalue. Since the change of variables $\bar{y} = A^\top y$ and $\bar{\theta} = B^\top \theta$ are isometries, we have

$$\mathcal{D}_H(\pi_{\bar{Y},\bar{\Theta}}, \tilde{\pi}_{\bar{Y},\bar{\Theta}})^2 = \mathcal{D}_H(\pi_{Y,\Theta}, \tilde{\pi}_{Y,\Theta}^{A,B})^2,$$

where $\tilde{\pi}_{Y,\Theta}^{A,B}(y, \theta) := \tilde{\pi}_{\bar{Y},\bar{\Theta}}(A^\top y, B^\top \theta)$. This concludes the proof.

C.5 Gaussian observation noise and Gaussian prior

We consider a belief parameter $\hat{\Theta} \in \mathbb{R}^{d_\Theta}$ equipped with a Gaussian prior $\mathcal{N}(\hat{\theta}_0, \Gamma)$, where $\hat{\theta}_0 \in \mathbb{R}^{d_\Theta}$ and $\Gamma \in \mathbb{R}^{d_\Theta \times d_\Theta}$. Given a smooth forward operator $\hat{\theta} \mapsto \hat{G}(\hat{\theta}) \in \mathbb{R}^{d_Y}$, we assume the observable information \hat{Y} follows $\mathcal{N}(\hat{G}(\hat{\Theta}), \Sigma)$. Then the joint density takes the form

$$\pi_{\hat{Y},\hat{\Theta}}(\hat{y}, \hat{\theta}) \propto \exp\left(-\frac{1}{2}\|\hat{y} - \hat{G}(\hat{\theta})\|_\Sigma^2 - \frac{1}{2}\|\hat{\theta} - \hat{\theta}_0\|_\Gamma^2\right), \quad (43)$$

where $\|v\|_\Gamma = \sqrt{v^\top \Gamma^{-1} v}$ is the matrix weighted norm. One can apply whitening transforms

$$Y = \Sigma^{-\frac{1}{2}} \hat{Y}, \quad \text{and} \quad \Theta = \Gamma^{-\frac{1}{2}} \hat{\Theta},$$

to obtain the joint density

$$\pi_{Y,\Theta}(y, \theta) = (2\pi)^{-\frac{d_Y+d_\Theta}{2}} \exp\left(-\frac{1}{2}\|y - G(\theta)\|_2^2 - \frac{1}{2}\|\theta - \theta_0\|_2^2\right), \quad (44)$$

where $G(\theta) := \hat{G}(\Gamma^{\frac{1}{2}}\theta)$ and $\theta_0 = \Gamma^{-\frac{1}{2}}\hat{\theta}_0$. Then, we construct a Gaussian reference density

$$\rho_{Y,\Theta}(y, \theta) = (2\pi)^{-\frac{d_Y+d_\Theta}{2}} \exp\left(-\frac{1}{2}\|y - G(\theta_0)\|_2^2 - \frac{1}{2}\|\theta - \theta_0\|_2^2\right),$$

where θ_0 is the prior mean. Then, we can express the joint density in the form of

$$\pi_{Y,\Theta}(y, \theta) = f(y, \theta) \rho_{Y,\Theta}(y, \theta),$$

where

$$f(y, \theta) = \exp\left(\frac{1}{2}\|y - G(\theta_0)\|_2^2 - \frac{1}{2}\|y - G(\theta)\|_2^2\right).$$

This leads to the pair of matrices

$$H_Y = \int \left(\nabla_y \log \frac{\pi_{Y,\Theta}}{\rho_{Y,\Theta}}\right) \left(\nabla_y \log \frac{\pi_{Y,\Theta}}{\rho_{Y,\Theta}}\right)^\top d\pi_{Y,\Theta} = \int \nabla_y f(y, \theta) \nabla_y f(y, \theta)^\top d\pi_{Y,\Theta}, \quad (45)$$

$$H_\Theta = \int \left(\nabla_\theta \log \frac{\pi_{Y,\Theta}}{\rho_{Y,\Theta}}\right) \left(\nabla_\theta \log \frac{\pi_{Y,\Theta}}{\rho_{Y,\Theta}}\right)^\top d\pi_{Y,\Theta} = \int \nabla_\theta f(y, \theta) \nabla_\theta f(y, \theta)^\top d\pi_{Y,\Theta}, \quad (46)$$

in which the gradients take the form

$$\nabla_y \log f(y, \theta) = G(\theta) - G(\theta_0), \quad \text{and} \quad \nabla_\theta \log f(y, \theta) = \nabla G(\theta)^\top (y - G(\theta)),$$

where $\theta \mapsto \nabla G(\theta) \in \mathbb{R}^{d_Y \times d_\Theta}$ is the Jacobian of the forward model. Since $\nabla_y \log f(y, \theta)$ is independent of y , the matrix H_Y can be expressed as

$$\begin{aligned} H_Y &= \int \nabla_y f(y, \theta) \nabla_y f(y, \theta)^\top \pi_{Y,\Theta}(y, \theta) dy d\theta \\ &= \int (G(\theta) - G(\theta_0)) (G(\theta) - G(\theta_0))^\top \left(\int \pi_{Y|\Theta}(y|\theta) dy\right) \pi_\Theta(\theta) d\theta \\ &= \int (G(\theta) - G(\theta_0)) (G(\theta) - G(\theta_0))^\top d\pi_\Theta. \end{aligned}$$

The matrix H_Θ can be expressed as

$$\begin{aligned} H_\Theta &= \int \nabla_\theta f(y, \theta) \nabla_\theta f(y, \theta)^\top d\pi_{Y,\Theta} \\ &= \int \nabla G(\theta)^\top \left(\int (y - G(\theta)) (y - G(\theta))^\top \pi_{Y|\Theta}(y|\theta) dy\right) \nabla G(\theta) \pi_\Theta(\theta) d\theta. \end{aligned}$$

Since $\int (y - G(\theta)) (y - G(\theta))^\top \pi_{Y|\Theta}(y|\theta) dy$ is the Fisher information of $\pi_{Y|\Theta}$, which is an identity matrix, we have

$$H_\Theta = \int \nabla G(\theta)^\top \nabla G(\theta) d\pi_\Theta.$$

D Proofs and additional details of Section 4

D.1 Proof of Proposition 3

Because the Hellinger distance satisfies the triangle inequality, we can write

$$\begin{aligned}
\mathcal{D}_H(p_{Y,\Theta}^{\ell+1}, \pi_{Y,\Theta}^{\ell+1}) &= \mathcal{D}_H((\mathcal{T}_\ell \circ \mathcal{Q}_{\ell+1})_{\#} \rho_{Y,\Theta}, \pi_{Y,\Theta}^{\ell+1}) \\
&= \mathcal{D}_H((\mathcal{Q}_{\ell+1})_{\#} \rho_{Y,\Theta}, \mathcal{T}_\ell^{\#} \pi_{Y,\Theta}^{\ell+1}) \\
&\stackrel{(17)}{\leq} \omega \mathcal{D}_H(p_{Y,\Theta}^{\ell}, \pi_{Y,\Theta}^{\ell+1}) \\
&\leq \omega \left(\mathcal{D}_H(p_{Y,\Theta}^{\ell}, \pi_{Y,\Theta}^{\ell}) + \mathcal{D}_H(\pi_{Y,\Theta}^{\ell}, \pi_{Y,\Theta}^{\ell+1}) \right) \\
&\stackrel{(18)}{\leq} \omega \left(\mathcal{D}_H(p_{Y,\Theta}^{\ell}, \pi_{Y,\Theta}^{\ell}) + \eta(L) \right),
\end{aligned}$$

for any $0 \leq \ell < L$. A direct recurrence yields

$$\begin{aligned}
\mathcal{D}_H(p_{Y,\Theta}^L, \pi_{Y,\Theta}^L) &\leq \omega^L \mathcal{D}_H(p_{Y,\Theta}^0, \pi_{Y,\Theta}^0) + \omega^L \eta(L) + \dots + \omega \eta(L) \\
&\leq \omega^{L+1} \eta(L) + \omega^L \eta(L) + \dots + \omega \eta(L) \\
&\leq \frac{\omega}{1-\omega} \eta(L),
\end{aligned}$$

which concludes the proof. \square

D.2 Bridging densities with uniformly spaced temperatures

Proposition 3 reveals that controlling the Hellinger distances between the bridging densities is one of the keys to ensure the accuracy of DIRT. Using the tempered pdf $\pi_{Y,\Theta}^{\ell} \propto \varphi_{Y,\Theta}^{\beta_{\ell}} \rho_{Y,\Theta}$ as the example, we demonstrate in Lemma 5 that under mild technical assumptions, the Hellinger distance between $\pi_{Y,\Theta}^{\ell}$ and $\pi_{Y,\Theta}^{\ell+1}$ is bounded by $\mathcal{O}(\beta_{\ell+1} - \beta_{\ell})$. This ensures that the uniformly spaced temperatures $\beta_{\ell} = \ell/L$ yields controlled Hellinger distances of the form of $\mathcal{D}_H(\pi_{Y,\Theta}^{\ell}, \pi_{Y,\Theta}^{\ell+1}) = \mathcal{O}(1/L)$.

Lemma 5. *We denote the supremum of $\log \varphi_{Y,\Theta}$, the mean and the second moment of $\log \rho_{Y,\Theta}$ with respect to $\rho_{Y,\Theta}$ by*

$$c_{\varphi} := \sup_{y,\theta} \log \varphi_{Y,\Theta}, \quad m_{\varphi} := \int \log \varphi_{Y,\Theta} d\rho_{Y,\Theta}, \quad \text{and} \quad V_{\varphi} := \int (\log \varphi_{Y,\Theta})^2 d\rho_{Y,\Theta},$$

respectively. Suppose $c_{\varphi} < \infty$ and $V_{\varphi} < \infty$. Considering the temperatures of adjacent levels satisfy $\beta_{\ell+1} = \beta_{\ell} + \Delta$ where $\Delta > 0$, the Hellinger distance between $\pi_{Y,\Theta}^{\ell} \propto \varphi_{Y,\Theta}^{\beta_{\ell}} \rho_{Y,\Theta}$ and $\pi_{Y,\Theta}^{\ell+1} \propto \varphi_{Y,\Theta}^{\beta_{\ell} + \Delta} \rho_{Y,\Theta}$ satisfies

$$\mathcal{D}_H(\pi_{Y,\Theta}^{\ell}, \pi_{Y,\Theta}^{\ell+1}) \leq \Delta C,$$

for any sequence of finite temperatures, where $C = C(c_{\varphi}, m_{\varphi}, V_{\varphi})$ is a constant independent of Δ .

Proof. We define the normalized pdfs

$$\pi_{Y,\Theta}^{\ell} = \frac{1}{z_{\ell}} \varphi_{Y,\Theta}^{\beta_{\ell}} \rho_{Y,\Theta} \quad \text{and} \quad \pi_{Y,\Theta}^{\ell+1} = \frac{1}{z_{\ell+1}} \varphi_{Y,\Theta}^{\beta_{\ell} + \Delta} \rho_{Y,\Theta},$$

where $z_{\ell} = \int \varphi_{Y,\Theta}^{\beta_{\ell}} d\rho_{Y,\Theta}$ and $z_{\ell+1} = \int \varphi_{Y,\Theta}^{\beta_{\ell} + \Delta} d\rho_{Y,\Theta}$. Applying Jensen's inequality, the mean m_{φ} satisfies $|m_{\varphi}| \leq \sqrt{V_{\varphi}} < \infty$, and we have the following lower bound on the normalizing constant

$$z_{\ell} = \exp \left(\log \left(\int \varphi_{Y,\Theta}^{\beta_{\ell}} d\rho_{Y,\Theta} \right) \right) \geq \exp \left(\int \log \varphi_{Y,\Theta}^{\beta_{\ell}} d\rho_{Y,\Theta} \right) = \exp(m_{\varphi} \beta_{\ell}) > 0, \quad (47)$$

for any finite β_{ℓ} . The difference between the normalizing constants has the following upper bound

$$|z_{\ell} - z_{\ell+1}| = \left| \int \left(\sqrt{\varphi_{Y,\Theta}^{\beta_{\ell}}} - \sqrt{\varphi_{Y,\Theta}^{\beta_{\ell} + \Delta}} \right) \left(\sqrt{\varphi_{Y,\Theta}^{\beta_{\ell}}} + \sqrt{\varphi_{Y,\Theta}^{\beta_{\ell} + \Delta}} \right) d\rho_{Y,\Theta} \right|$$

$$\begin{aligned}
&\leq \left(\int \left(\sqrt{\varphi_{Y,\Theta}^{\beta_\ell}} - \sqrt{\varphi_{Y,\Theta}^{\beta_\ell+\Delta}} \right)^2 d\rho_{Y,\Theta} \right)^{\frac{1}{2}} \left(\int \left(\sqrt{\varphi_{Y,\Theta}^{\beta_\ell}} + \sqrt{\varphi_{Y,\Theta}^{\beta_\ell+\Delta}} \right)^2 d\rho_{Y,\Theta} \right)^{\frac{1}{2}} \\
&\leq \left(\int \left(\sqrt{\varphi_{Y,\Theta}^{\beta_\ell}} - \sqrt{\varphi_{Y,\Theta}^{\beta_\ell+\Delta}} \right)^2 d\rho_{Y,\Theta} \right)^{\frac{1}{2}} \left(\sqrt{\int \varphi_{Y,\Theta}^{\beta_\ell} d\rho_{Y,\Theta}} + \sqrt{\int \varphi_{Y,\Theta}^{\beta_\ell+\Delta} d\rho_{Y,\Theta}} \right) \\
&= \left(\int \left(\sqrt{\varphi_{Y,\Theta}^{\beta_\ell}} - \sqrt{\varphi_{Y,\Theta}^{\beta_\ell+\Delta}} \right)^2 d\rho_{Y,\Theta} \right)^{\frac{1}{2}} (\sqrt{z_\ell} + \sqrt{z_{\ell+1}}). \tag{48}
\end{aligned}$$

Applying the identity $|z_\ell - z_{\ell+1}| = |\sqrt{z_\ell} - \sqrt{z_{\ell+1}}|(\sqrt{z_\ell} + \sqrt{z_{\ell+1}})$, the inequality in (48) yields

$$|\sqrt{z_\ell} - \sqrt{z_{\ell+1}}| \leq \left(\int \left(\sqrt{\varphi_{Y,\Theta}^{\beta_\ell}} - \sqrt{\varphi_{Y,\Theta}^{\beta_\ell+\Delta}} \right)^2 d\rho_{Y,\Theta} \right)^{\frac{1}{2}}. \tag{49}$$

This way, the Hellinger distance satisfies

$$\begin{aligned}
&\mathcal{D}_H(\pi_{Y,\Theta}^\ell, \pi_{Y,\Theta}^{\ell+1}) \\
&= \frac{1}{\sqrt{2}} \left(\int \left(\sqrt{\frac{\varphi_{Y,\Theta}^{\beta_\ell}}{z_\ell}} - \sqrt{\frac{\varphi_{Y,\Theta}^{\beta_\ell+\Delta}}{z_{\ell+1}}} \right)^2 d\rho_{Y,\Theta} \right)^{\frac{1}{2}} \\
&= \frac{1}{\sqrt{2z_\ell}} \left(\int \left(\sqrt{\varphi_{Y,\Theta}^{\beta_\ell}} - \sqrt{\varphi_{Y,\Theta}^{\beta_\ell+\Delta}} \sqrt{\frac{z_\ell}{z_{\ell+1}}} \right)^2 d\rho_{Y,\Theta} \right)^{\frac{1}{2}} \\
&= \frac{1}{\sqrt{2z_\ell}} \left(\int \left(\sqrt{\varphi_{Y,\Theta}^{\beta_\ell}} - \sqrt{\varphi_{Y,\Theta}^{\beta_\ell+\Delta}} + \sqrt{\varphi_{Y,\Theta}^{\beta_\ell+\Delta}} - \sqrt{\varphi_{Y,\Theta}^{\beta_\ell+\Delta}} \sqrt{\frac{z_\ell}{z_{\ell+1}}} \right)^2 d\rho_{Y,\Theta} \right)^{\frac{1}{2}} \\
&\leq \frac{1}{\sqrt{2z_\ell}} \left(\int \left(\sqrt{\varphi_{Y,\Theta}^{\beta_\ell}} - \sqrt{\varphi_{Y,\Theta}^{\beta_\ell+\Delta}} \right)^2 d\rho_{Y,\Theta} \right)^{\frac{1}{2}} + \frac{1}{\sqrt{2z_\ell}} \left(\int \varphi_{Y,\Theta}^{\beta_\ell+\Delta} \left(1 - \sqrt{\frac{z_\ell}{z_{\ell+1}}} \right)^2 d\rho_{Y,\Theta} \right)^{\frac{1}{2}} \\
&= \frac{1}{\sqrt{2z_\ell}} \left(\int \left(\sqrt{\varphi_{Y,\Theta}^{\beta_\ell}} - \sqrt{\varphi_{Y,\Theta}^{\beta_\ell+\Delta}} \right)^2 d\rho_{Y,\Theta} \right)^{\frac{1}{2}} + \frac{|\sqrt{z_{\ell+1}} - \sqrt{z_\ell}|}{\sqrt{2z_\ell}} \\
&\stackrel{(49)}{\leq} \sqrt{\frac{2}{z_\ell}} \left(\int \left(\sqrt{\varphi_{Y,\Theta}^{\beta_\ell}} - \sqrt{\varphi_{Y,\Theta}^{\beta_\ell+\Delta}} \right)^2 d\rho_{Y,\Theta} \right)^{\frac{1}{2}}. \tag{50}
\end{aligned}$$

Applying Hölder's inequality, we have

$$\mathcal{D}_H(\pi_{Y,\Theta}^\ell, \pi_{Y,\Theta}^{\ell+1}) \leq \left(\frac{2 \sup_{y,\theta} (\varphi_{Y,\Theta}^{\beta_\ell})}{z_\ell} \int \left(1 - \varphi_{Y,\Theta}^{\Delta/2} \right)^2 d\rho_{Y,\Theta} \right)^{\frac{1}{2}} \tag{51}$$

$$= \left(\frac{2 \exp(\beta_\ell c_\varphi)}{z_\ell} \int \left(1 - \varphi_{Y,\Theta}^{\Delta/2} \right)^2 d\rho_{Y,\Theta} \right)^{\frac{1}{2}}. \tag{52}$$

By the Lipschitz continuity of the exponential function in the domain $(-\infty, a]$ for $a < \infty$, we have

$$\left| 1 - \varphi_{Y,\Theta}^{\Delta/2} \right| = \left| \exp(0) - \exp\left(\frac{\Delta}{2} \log \varphi_{Y,\Theta}\right) \right| \leq \exp\left(\max\left(0, \frac{c_\varphi \Delta}{2}\right)\right) \left| \frac{\Delta}{2} \log \varphi_{Y,\Theta} - 0 \right|,$$

which leads to

$$\left(1 - \varphi_{Y,\Theta}^{\Delta/2} \right)^2 \leq \frac{\Delta^2 \exp(\max(0, c_\varphi \Delta))}{4} (\log \varphi_{Y,\Theta})^2.$$

Substituting the above inequality into (52), we have

$$\mathcal{D}_H(\pi_{Y,\Theta}^\ell, \pi_{Y,\Theta}^{\ell+1}) \leq \left(\frac{\Delta^2 \exp(\max(c_\varphi \beta_\ell, c_\varphi \beta_{\ell+1}))}{2z_\ell} \int (\log \varphi_{Y,\Theta})^2 d\rho_{Y,\Theta} \right)^{\frac{1}{2}}$$

$$\begin{aligned}
&\stackrel{(47)}{\leq} \left(\frac{\Delta^2 \exp(\max(c_\varphi \beta_\ell, c_\varphi \beta_{\ell+1}))}{2 \exp(m_\varphi \beta_\ell)} \right)^{\frac{1}{2}} \left(\int (\log \varphi_{Y,\Theta})^2 d\rho_{Y,\Theta} \right)^{\frac{1}{2}} \\
&= \Delta \left(\frac{1}{2} \exp(-m_\varphi \beta_\ell + \max(c_\varphi \beta_\ell, c_\varphi \beta_{\ell+1})) V_\varphi \right)^{\frac{1}{2}}.
\end{aligned}$$

Thus, the Hellinger distance satisfies

$$\mathcal{D}_H(\pi_{Y,\Theta}^\ell, \pi_{Y,\Theta}^{\ell+1}) \leq \Delta \left(\frac{1}{2} V_\varphi \sup_\ell \exp(-m_\varphi \beta_\ell) \sup_\ell \exp(c_\varphi \beta_\ell) \right)^{\frac{1}{2}},$$

which concludes the proof. \square

D.3 Adaptive temperature selection in DIRT

We can also employ the adaptive tempering method introduced in the sequential Monte Carlo literature, e.g., [2, 23, 24, 32, 39, 46], to provide a more precise control of the temperatures during the DIRT construction. We want to control the Hellinger distance between two bridging densities, so that it satisfies

$$\mathcal{D}_H(\pi_{Y,\Theta}^\ell, \pi_{Y,\Theta}^{\ell+1}) \approx \eta$$

for some $\eta \in [0, 1)$. Since the Hellinger distance can be expressed as

$$\mathcal{D}_H(\pi_{Y,\Theta}^\ell, \pi_{Y,\Theta}^{\ell+1}) = \left(\frac{1}{2} \int \left(\sqrt{\frac{\pi_{Y,\Theta}^{\ell+1}}{\pi_{Y,\Theta}^\ell}} - 1 \right)^2 d\pi_{Y,\Theta}^\ell \right)^{\frac{1}{2}} = \frac{1}{\sqrt{2}} \left(1 - \sqrt{\frac{z_\ell}{z_{\ell+1}}} \int \varphi_{Y,\Theta}^{\Delta/2} d\pi_{Y,\Theta}^\ell \right)^{\frac{1}{2}}. \quad (53)$$

We can utilize the current composition of transport maps \mathcal{T}_ℓ to estimate the Hellinger distance in the adaptive temperature selection. The pushforward density $p_{Y,\Theta}^\ell = (\mathcal{T}_\ell)_\# \rho_{Y,\Theta}$, which is an approximation to $\pi_{Y,\Theta}^\ell$, defines importance sampling formulas

$$\frac{z_{\ell+1}}{z_\ell} = \int \varphi_{Y,\Theta}^\Delta d\pi_{Y,\Theta}^\ell = \int \varphi_{Y,\Theta}^\Delta \frac{\pi_{Y,\Theta}^\ell}{p_{Y,\Theta}^\ell} dp_{Y,\Theta}^\ell, \quad (54)$$

$$\int \varphi_{Y,\Theta}^{\Delta/2} d\pi_{Y,\Theta}^\ell = \int \varphi_{Y,\Theta}^{\Delta/2} \frac{\pi_{Y,\Theta}^\ell}{p_{Y,\Theta}^\ell} dp_{Y,\Theta}^\ell. \quad (55)$$

One can draw samples $\{Y_\ell^i, \Theta_\ell^i\}_{i=1}^N \sim p_{Y,\Theta}^\ell$ and compute

$$F_\ell^i = \log \varphi_{Y,\Theta}(Y_\ell^i, \Theta_\ell^i), \quad (56)$$

$$\begin{aligned}
W_\ell^i &= \log \pi_{Y,\Theta}^\ell(Y_\ell^i, \Theta_\ell^i) - \log p_{Y,\Theta}^\ell(Y_\ell^i, \Theta_\ell^i) \\
&= \beta_\ell F_\ell^i + \log \rho_{Y,\Theta}(Y_\ell^i, \Theta_\ell^i) - \log p_{Y,\Theta}^\ell(Y_\ell^i, \Theta_\ell^i)
\end{aligned} \quad (57)$$

Then, the formulas in (53)–(55) lead to the estimated Hellinger distance

$$\mathcal{D}_H(\pi_{Y,\Theta}^\ell, \pi_{Y,\Theta}^{\ell+1}) \approx D(\Delta, \ell, N) := \frac{1}{\sqrt{2}} \left(1 - \frac{\sum_{i=1}^N \exp(\frac{\Delta}{2} F_\ell^i + W_\ell^i)}{(N \sum_{i=1}^N \exp(\Delta F_\ell^i + W_\ell^i))^{1/2}} \right)^{\frac{1}{2}}, \quad (58)$$

which is used in Algorithm 4 to adaptively identify the next bridging density in the DIRT construction. Note that the formula in (58) is shift-invariant to W_ℓ^i .

E Further numerical tests

E.1 Elasticity model

In Figure 4 we investigate the Hellinger error between the conditional DIRT approximation and the exact posterior on a given reduced subspace for different TT ranks, tempering parameters, and orders of variables. We observe that the approximation error of TT decreases asymptotically with

Algorithm 4 DIRT with adaptive temperature selection.

- 1: **procedure** DIRT($\rho_{Y,\Theta}, \varphi_{Y,\Theta}, \omega, \eta$)
 - 2: Call SIRT($\rho_{Y,\Theta}, \pi_{Y,\Theta}^0, \omega\eta$) to get the first layer \mathcal{Q}_0 and initialize $\mathcal{T}_0 = \mathcal{Q}_0$
 - 3: **while** $\beta_\ell < 1$ **do**
 - 4: Set $\ell = \ell + 1$.
 - 5: Call NEXTBETA($\rho_{Y,\Theta}, \varphi_{Y,\Theta}, \beta_{\ell-1}, \mathcal{T}_{\ell-1}, \eta$) to get a new β_ℓ .
 - 6: Call SIRT($\rho_{Y,\Theta}, \mathcal{T}_\ell^\# \pi_{Y,\Theta}^{\ell+1}, \omega\eta$) to get the next layer $\mathcal{Q}_{\ell+1}$.
 - 7: Update $\mathcal{T}_{\ell+1} = \mathcal{T}_\ell \circ \mathcal{Q}_{\ell+1}$.
 - 8: **end while**
 - 9: Set $L = \ell$.
 - 10: **return** the map \mathcal{T}_L such that $p_{Y,\Theta} = (\mathcal{T}_L)_\# \rho_{Y,\Theta}$ approximates $\pi_{Y,\Theta}^L = \pi_{Y,\Theta}$
 - 11: **end procedure**

 - 12: **procedure** NEXTBETA($\rho_{Y,\Theta}, \varphi_{Y,\Theta}, \beta, \mathcal{T}, \eta$)
 - 13: Draw samples $(Y_\ell^i, \Theta_\ell^i) = \mathcal{T}(U_i)$ where $U_i \sim \rho_{Y,\Theta}$ for $i = 1, \dots, N$.
 - 14: Find Δ such that $D(\Delta, \ell, N) = \eta$. where $D(\Delta, \ell, N)$ is given in (58).
 - 15: **return** $\beta' = \min(\beta + \Delta, 1)$.
 - 16: **end procedure**
-

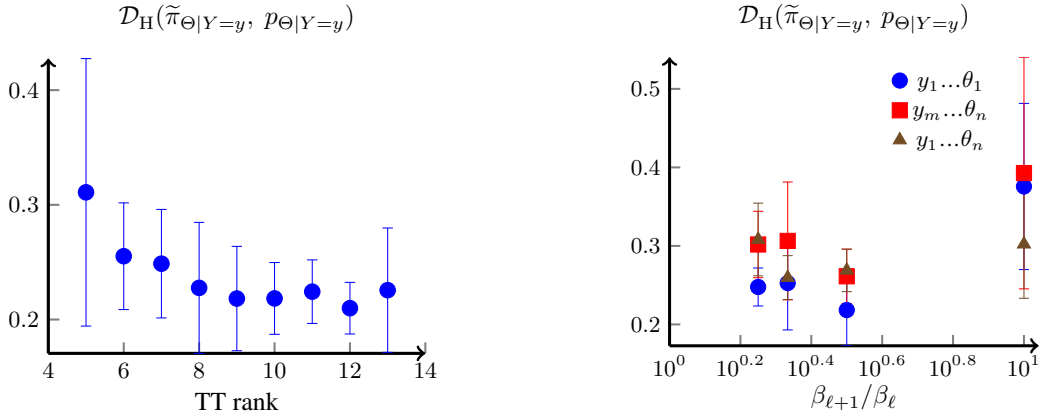


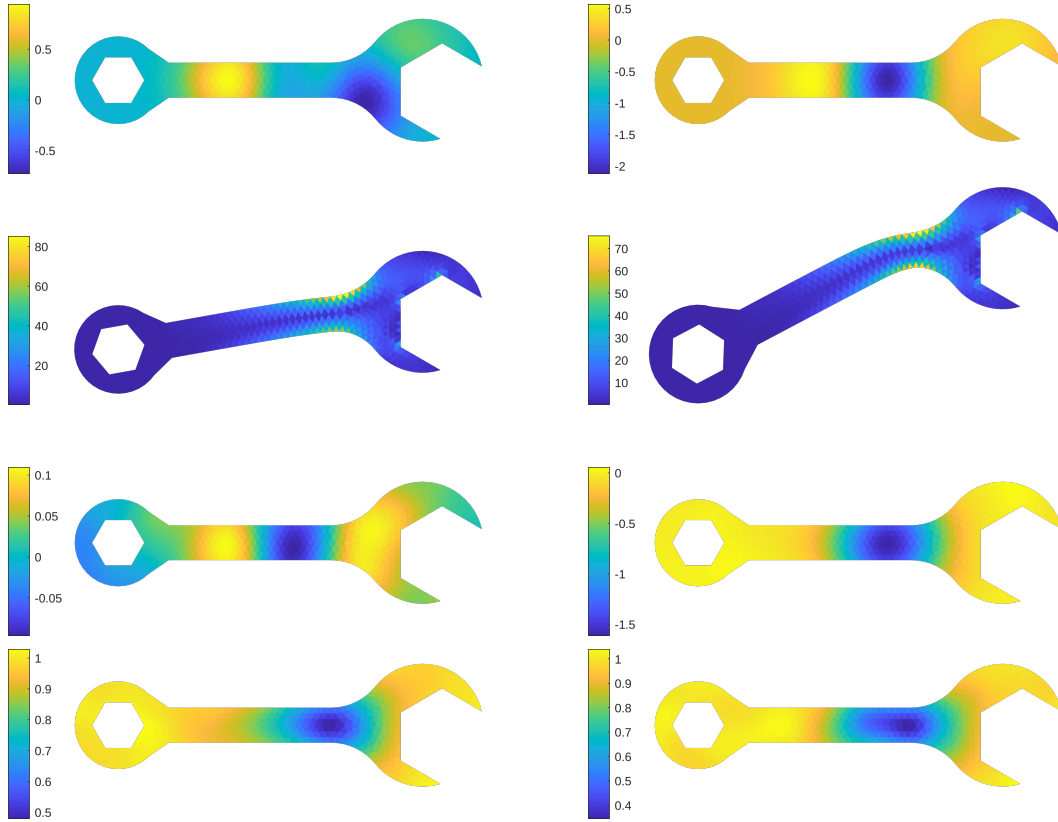
Figure 4: Wrenchmark: Hellinger distances (mean \pm std over 10 data samples) between the conditional DIRT approximation and the exact posterior with reduced dimensions $n_\Theta = 10$, $n_Y = 13$. Left: TT rank varies and $\beta_{\ell+1}/\beta_\ell = \sqrt{10}$ is fixed. Right: $\beta_{\ell+1}/\beta_\ell$ varies and TT ranks are fixed to 9.

increasing TT ranks. However, the error stops decaying after rank 9. This may suggest that one needs to further increase the resolution of the discretization grid in constructing TT (cf. Section B.2) if further accuracy improvement is desired. Fixing the TT ranks to 9, we observe that among different sequences of temperatures, the sequence with the ratio $\beta_{\ell+1}/\beta_\ell = \sqrt{10}$ gives the best accuracy.

In Figure 5 (top) we show the logarithm of the Young’s modulus $\log E$ and the von Mises stress produced from two samples from the prior (in the reduced space with $n_\Theta = 7$). These samples are treated as the “ground truth” to simulate the observation data (in the reduced space with $n_Y = 13$). In the remaining rows of Figure 5, we compute posterior mean and standard deviation of $\log E$ conditioned on those “ground truth” data. Finally, the last row of Figure 5 shows the accuracy of DIRT and dimension reduction.

E.2 Elliptic PDE with Besov prior

In Figure 6 we plot two synthetic “ground truth” samples of the logarithm of the diffusion coefficient, and the corresponding solution used to generate the observation data. We reduce the state dimension



$$\frac{\mathcal{D}_H(\tilde{\pi}, p)}{0.172} \mid \frac{\mathcal{D}_H(\pi, \tilde{\pi})}{0.151}$$

$$\frac{\mathcal{D}_H(\tilde{\pi}, p)}{0.298} \mid \frac{\mathcal{D}_H(\pi, \tilde{\pi})}{0.289}$$

Figure 5: Top two rows: two prior realizations of $\log E$ (log-Young’s modulus) and the von Mises stress. Rows 3 and 4: mean and standard deviation of $\log E$ with respect to the posterior conditioned on the data produced from the corresponding prior realizations. Bottom row: Hellinger-distance errors between the conditional DIRT approximation and the exact reduced posterior, and between reduced and full posteriors.

to $n_\Theta = 12$. The last row of Figure 6 shows the accuracy of DIRT and dimension reduction. In Figure 7 we compute posterior mean and standard deviation of $\log \kappa$ conditioned on those “ground truth” data. We observe that the inferred posterior mean coefficient reproduces the observed solution.

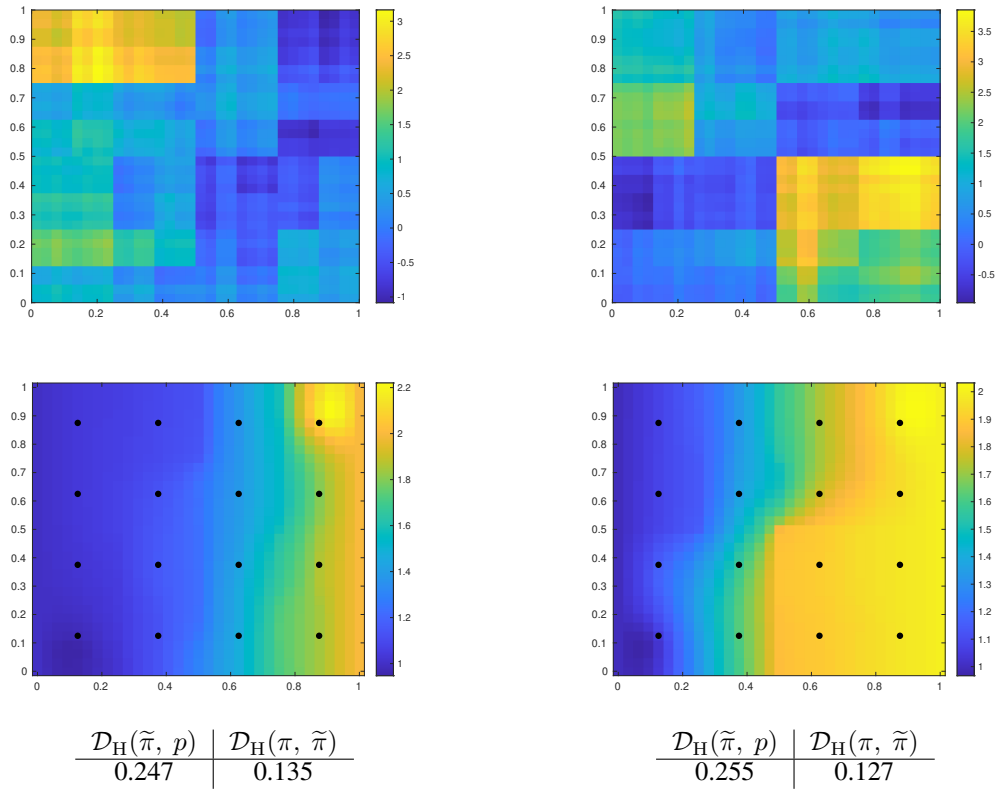


Figure 6: Top two rows: two prior realizations of $\log \kappa$ and the solution u . Black dots show the locations of the observations. Bottom row: Hellinger-distance errors between the conditional DIRT approximation and the exact reduced posterior, and between reduced and full posteriors.

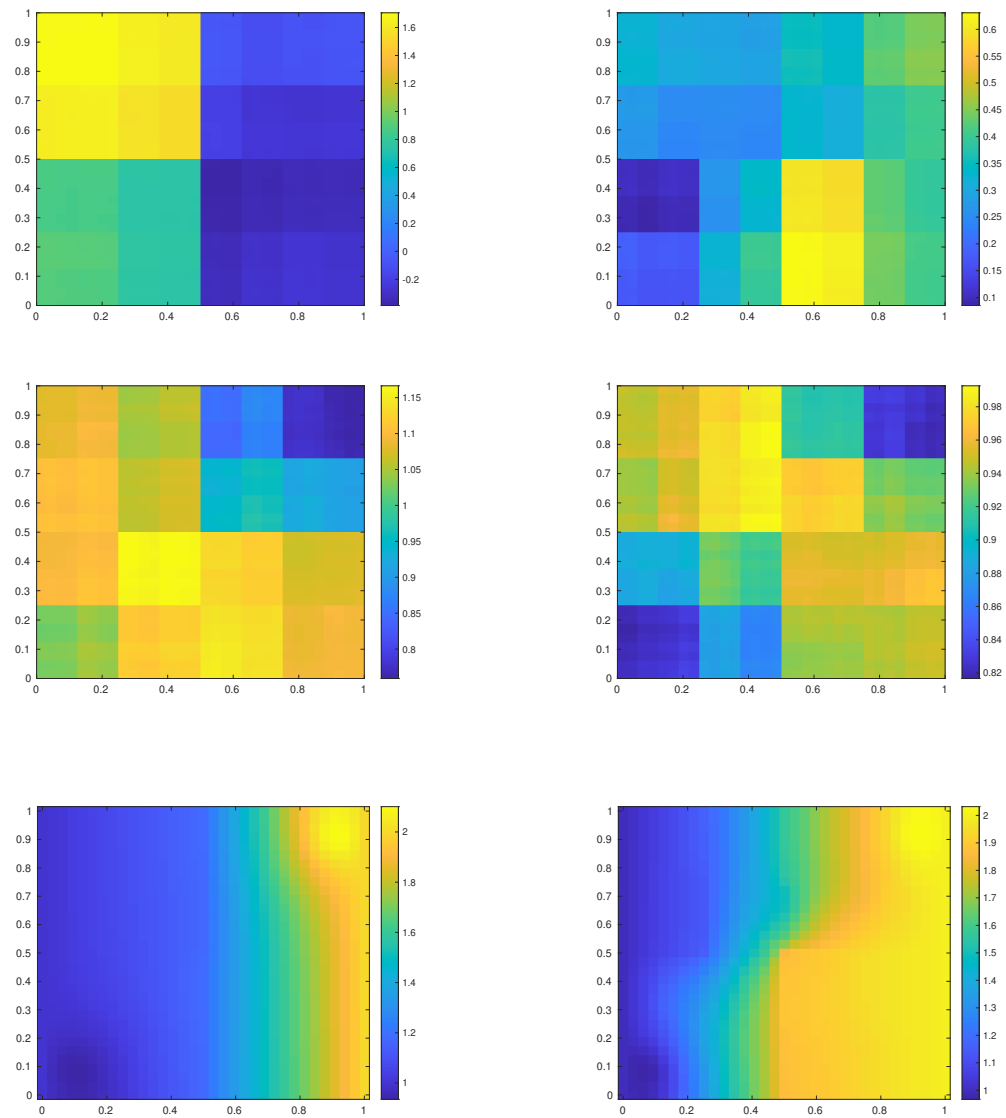


Figure 7: Top two rows: mean and standard deviation of $\log \kappa$ with respect to the posterior conditioned on the data produced from the corresponding prior realizations. Bottom row: the solution computed from mean $\log \kappa$.

References

- [1] Ricardo Baptista, Olivier Zahm, and Youssef Marzouk. An adaptive transport framework for joint and conditional density estimation. *arXiv preprint arXiv:2009.10303*, 2020.
- [2] Alexandros Beskos, Ajay Jasra, Nikolas Kantas, Alexandre Thiery, et al. On the convergence of adaptive sequential monte carlo methods. *Annals of Applied Probability*, 26(2):1111–1146, 2016.
- [3] Daniele Bigoni, Allan P Engsig-Karup, and Youssef M Marzouk. Spectral tensor-train decomposition. *SIAM Journal on Scientific Computing*, 38(4):A2405–A2439, 2016.
- [4] Michael C. Brennan, Daniele Bigoni, Olivier Zahm, Alessio Spantini, and Youssef Marzouk. Greedy inference with structure-exploiting lazy maps. In *Advances in Neural Information Processing Systems*, volume 33, pages 8330–8342, 2020.
- [5] S. Brooks, A. Gelman, G. Jones, and X. L. Meng, editors. *Handbook of Markov Chain Monte Carlo*. Taylor & Francis, 2011.
- [6] Anthony Caterini, Rob Cornish, Dino Sejdinovic, and Arnaud Doucet. Variational inference with continuously-indexed normalizing flows. *arXiv preprint arXiv:2007.05426*, 2020.
- [7] Ricky T. Q. Chen, Jens Behrmann, David K Duvenaud, and Joern-Henrik Jacobsen. Residual flows for invertible generative modeling. In H. Wallach, H. Larochelle, A. Beygelzimer, F. d’ Alché-Buc, E. Fox, and R. Garnett, editors, *Advances in Neural Information Processing Systems*, volume 32. Curran Associates, Inc., 2019.
- [8] Herman Chernoff. A note on an inequality involving the normal distribution. *The Annals of Probability*, pages 533–535, 1981.
- [9] N. Chopin. A sequential particle filter method for static models. *Biometrika*, 89(3):539–552, 2002.
- [10] Rob Cornish, Anthony Caterini, George Deligiannidis, and Arnaud Doucet. Relaxing bijectivity constraints with continuously indexed normalising flows. In Hal Daumé III and Aarti Singh, editors, *Proceedings of the 37th International Conference on Machine Learning*, volume 119 of *Proceedings of Machine Learning Research*, pages 2133–2143. PMLR, 13–18 Jul 2020.
- [11] Tiangang Cui and Sergey Dolgov. Deep composition of tensor trains using squared inverse rosenblatt transports. *arXiv preprint arXiv:2007.06968*, 2020.
- [12] Tiangang Cui and Xin T Tong. A unified performance analysis of likelihood-informed subspace methods. *arXiv preprint arXiv:2101.02417*, 2021.
- [13] Tiangang Cui and Olivier Zahm. Data-free likelihood-informed dimension reduction of bayesian inverse problems. *Inverse Problems*, 37(4):045009, 2021.
- [14] Masoumeh Dashti, Stephen Harris, and Andrew Stuart. Besov priors for Bayesian inverse problems. *Inverse Problems & Imaging*, 6(2):183, 2012.
- [15] P. Del Moral, A. Doucet, and A. Jasra. Sequential Monte Carlo samplers. *Journal of the Royal Statistical Society: Series B (Statistical Methodology)*, 68(3):411–436, 2006.
- [16] Sergey Dolgov, Karim Anaya-Izquierdo, Colin Fox, and Robert Scheichl. Approximation and sampling of multivariate probability distributions in the tensor train decomposition. *Statistics and Computing*, 30(3):603–625, 2020.
- [17] Sergey V Dolgov and Dmitry V Savostyanov. Alternating minimal energy methods for linear systems in higher dimensions. *SIAM Journal on Scientific Computing*, 36(5):A2248–A2271, 2014.
- [18] Andrew Gelman and Xiao-Li Meng. Simulating normalizing constants: From importance sampling to bridge sampling to path sampling. *Statistical Science*, pages 163–185, 1998.
- [19] Sergei A Goreinov, Nikolai Leonidovich Zamarashkin, and Eugene E Tyrtysnikov. Pseudo-skeleton approximations by matrices of maximal volume. *Mathematical Notes*, 62(4):515–519, 1997.
- [20] Alex Gorodetsky, Sertac Karaman, and Youssef M Marzouk. A continuous analogue of the tensor-train decomposition. *Computer Methods in Applied Mechanics and Engineering*, 347:59–84, 2019.
- [21] Michael Griebel and Helmut Harbrecht. Analysis of tensor approximation schemes for continuous functions. *arXiv preprint arXiv:1903.04234*, 2019.
- [22] Wolfgang Hackbusch. *Tensor spaces and numerical tensor calculus*, volume 42. Springer Science & Business Media, 2012.
- [23] Ajay Jasra, David A Stephens, Arnaud Doucet, and Theodoros Tsagaris. Inference for lévy-driven stochastic volatility models via adaptive sequential monte carlo. *Scandinavian Journal of Statistics*, 38(1):1–22, 2011.
- [24] Nikolas Kantas, Alexandros Beskos, and Ajay Jasra. Sequential monte carlo methods for high-dimensional inverse problems: A case study for the navier–stokes equations. *SIAM/ASA Journal on Uncertainty Quantification*, 2(1):464–489, 2014.

- [25] Tamara G Kolda and Brett W Bader. Tensor decompositions and applications. *SIAM Review*, 51(3):455–500, 2009.
- [26] Nikola Kovachki, Ricardo Baptista, Bamdad Hosseini, and Youssef Marzouk. Conditional sampling with monotone gans. *arXiv preprint arXiv:2006.06755*, 2020.
- [27] J. Kruse, G. Detommaso, R. Scheichl, and U. Koethe. HINT: Hierarchical invertible neural transport for density estimation and Bayesian inference. In *The AAAI Conference on Artificial Intelligence (AAAI)*, page to appear, 2021.
- [28] Remi R Lam, Olivier Zahm, Youssef M Marzouk, and Karen E Willcox. Multifidelity dimension reduction via active subspaces. *SIAM Journal on Scientific Computing*, 42(2):A929–A956, 2020.
- [29] Matti Lassas, Eero Saksman, and Samuli Siltanen. Discretization-invariant Bayesian inversion and Besov space priors. *Inverse problems and imaging*, 3(1):87–122, 2009.
- [30] Jun S Liu. *Monte Carlo strategies in scientific computing*. Springer Science & Business Media, 2008.
- [31] Michael W Mahoney and Petros Drineas. CUR matrix decompositions for improved data analysis. *Proceedings of the National Academy of Sciences*, 106(3):697–702, 2009.
- [32] Aaron Myers, Alexandre H Thiéry, Kainan Wang, and Tan Bui-Thanh. Sequential ensemble transform for bayesian inverse problems. *Journal of Computational Physics*, 427:110055, 2021.
- [33] Radford M Neal. Sampling from multimodal distributions using tempered transitions. *Statistics and computing*, 6(4):353–366, 1996.
- [34] Ivan Oseledets and Eugene Tyrtyshnikov. TT-cross approximation for multidimensional arrays. *Linear Algebra and its Applications*, 432(1):70–88, 2010.
- [35] Felix Otto and Cédric Villani. Generalization of an inequality by talagrand and links with the logarithmic sobolev inequality. *Journal of Functional Analysis*, 173(2):361–400, 2000.
- [36] George Papamakarios, Eric Nalisnick, Danilo Jimenez Rezende, Shakir Mohamed, and Balaji Lakshminarayanan. Normalizing flows for probabilistic modeling and inference. *arXiv preprint arXiv:1912.02762*, 2019.
- [37] Matthew D Parno and Youssef M Marzouk. Transport map accelerated Markov chain Monte Carlo. *SIAM/ASA Journal on Uncertainty Quantification*, 6(2):645–682, 2018.
- [38] Danilo Jimenez Rezende and Shakir Mohamed. Variational inference with normalizing flows. *arXiv preprint arXiv:1505.05770*, 2015.
- [39] Christian Schäfer and Nicolas Chopin. Sequential monte carlo on large binary sampling spaces. *Statistics and Computing*, 23(2):163–184, 2013.
- [40] Kathrin Smetana and Olivier Zahm. Randomized residual-based error estimators for the proper generalized decomposition approximation of parametrized problems. *International Journal for Numerical Methods in Engineering*, 121(23):5153–5177, 2020.
- [41] Alessio Spantini, Ricardo Baptista, and Youssef Marzouk. Coupling techniques for nonlinear ensemble filtering. *arXiv preprint arXiv:1907.00389*, 2019.
- [42] Robert H Swendsen and Jian-Sheng Wang. Replica Monte Carlo simulation of spin-glasses. *Physical Review Letters*, 57(21):2607, 1986.
- [43] Esteban G Tabak and Cristina V Turner. A family of nonparametric density estimation algorithms. *Communications on Pure and Applied Mathematics*, 66(2):145–164, 2013.
- [44] Giulio Trigila and Esteban G Tabak. Data-driven optimal transport. *Communications on Pure and Applied Mathematics*, 69(4):613–648, 2016.
- [45] Olivier Zahm, Tiangang Cui, Kody Law, Alessio Spantini, and Youssef Marzouk. Certified dimension reduction in nonlinear Bayesian inverse problems. *arXiv preprint arXiv:1807.03712*, 2018.
- [46] Yan Zhou, Adam M Johansen, and John AD Aston. Toward automatic model comparison: an adaptive sequential monte carlo approach. *Journal of Computational and Graphical Statistics*, 25(3):701–726, 2016.